Coastal Protection and Restoration Authority
150 Terrace Avenue, Baton Rouge, LA 70802 | coastal@la.gov | www.coastal.la.gov

2017 Coastal Master Plan

Attachment C3-1: Sediment Distribution

Report: Final

Date: April 2017

Prepared By: Alex McCorquodale (University of New Orleans), Brady Couvillion (U.S. Geological Survey), Mark Dortch (Moffatt and Nichol), Angelina Freeman (Coastal Restoration and Protection Authority), Ehab Meselhe (The Water Institute of the Gulf), Denise Reed (The Water Institute of the Gulf), Ben Roth (The Water Institute of the Gulf), Jeff Shelden (Moffatt and Nichol), Gregg Snedden (U.S. Geological Survey), Hongqing Wang (U.S. Geological Survey), and Eric White (The Water Institute of the Gulf)

Coastal Protection and Restoration Authority

This document was prepared in support of the 2017 Coastal Master Plan being prepared by the Coastal Protection and Restoration Authority (CPRA). CPRA was established by the Louisiana Legislature in response to Hurricanes Katrina and Rita through Act 8 of the First Extraordinary Session of 2005. Act 8 of the First Extraordinary Session of 2005 expanded the membership, duties and responsibilities of CPRA and charged the new authority to develop and implement a comprehensive coastal protection plan, consisting of a master plan (revised every five years) and annual plans. CPRA's mandate is to develop, implement and enforce a comprehensive coastal protection and restoration master plan.

Suggested Citation:

McCorquodale, A., Couvillion, B., Dortch, Freeman, A., M., Meselhe, E., Reed, D., Roth, B., Shelden, J., Snedden, G., Wang, H., and White, E. (2017). *2017 Coastal Master Plan: Attachment C3-1: Sediment Distribution.* Version Final. (pp. 1-56). Baton Rouge, Louisiana: Coastal Protection and Restoration Authority.

Acknowledgements

This document was developed as part of a broader Model Improvement Plan in support of the 2017 Coastal Master Plan under the guidance of the Modeling Decision Team (MDT):

- The Water Institute of the Gulf (the Institute) - Ehab Meselhe, Alaina Grace, and Denise Reed
- Coastal Protection and Restoration Authority (CPRA) of Louisiana - Mandy Green, Angelina Freeman, and David Lindquist

The following people assisted with access and summaries of data used in this report:

- University of New Orleans - Dr. Ioannis Georgiou and John Filostrat
- South Carolina Department of Natural Resources - Andrew Tweel
- Louisiana State University - R. Eugene Turner

This effort was funded by CPRA of Louisiana under Cooperative Endeavor Agreement Number 2503-12-58, Task Order No. 03.

Executive Summary

This report describes the development of sediment distribution and morphology processes required to simulate the responses of the coastal area to the hydrological, meteorological and geological conditions over fifty years. A literature review was used as a basis for the proposed processes for the Integrated Compartment Model (ICM) for the 2017 Coastal Master Plan. These included: resuspension and transport of sand, silt, flocculated and particulate clay in open water; exchange of sediment between open water and marshes and sediment processes related to hurricanes. The contribution of wave energy to sediment distribution was also investigated.

In the ICM, resuspension for the silt and clay is based on excess bed shear (bed shear – critical shear) and consolidation time. The flocculation of clay is a function of the salinity. The sand accumulation rate in open water is related to the difference between the sand inflow and the sand transport capacity. The flow exchange between the open water and the marshes is described by the Kadlec-Knight formula. The sedimentation in the marshes is treated in two zones: near-shore and interior. No resuspension of sediment in the marshes occurs under non-hurricane conditions. During storm conditions the same processes erode and deposit sediment throughout the system with some limits applied to suspended sediment concentration and bed erosion.

Table of Contents

Coastal Protection and Restoration Authority ii

Acknowledgements iii

Executive Summary iv

List of Tables vi

List of Figures vi

List of Abbreviations viii

1.0 Introduction 1

2.0 Open Water Sediment Distribution Processes 5
2.1 Deposition of Suspended Sediments 6
2.1.1 Flocculation 8
2.2 Resuspension 12
2.2.1 Resuspension of Silt and Clay Particles 12
2.2.2 Bed Shear Stress 13
2.2.3 Resuspension of Sand Particles 17
2.3 Routing of Suspended Sediments 18
2.3.1 Link Adjustments 21
2.4 Open Water Processes 21
2.4.1 Mass Balance 21
2.4.2 Resuspension of Cohesive Sediments 22
2.4.3 Deposition of Sediments 22
2.4.4 Net Resuspension and Deposition of Cohesive Sediments 22
2.4.5 Net Resuspension and Deposition of Noncohesive Sediments 22
2.4.6 Delta Building 23
2.4.7 Link Adjustments 23

3.0 Exchange between Open Water and Marsh (Excluding Hurricanes) 24
3.1 Open Water-Marsh Exchange Modeling Approach 25

4.0 Sediment Processes in the Marsh Areas (Excluding Hurricanes) 26
4.1 Modeling Approach for Marsh Sediment Delivery 29

5.0 Sediment Processes in the Marsh Areas (During Hurricanes) 29
5.1 Context 29
5.1.1 Sources 30
5.1.2 Processes 30
5.1.3 Magnitude and Distribution 30
5.1.4 Controlling Factors 30
5.1.5 Calculating Sediment Contribution 31
5.2 Approach Adopted 31

6.0 Contribution of Marsh Edge Erosion to the Sediment Mass Balance 32

7.0 Sediment Distribution Code Organization 32

8.0 Code Testing 36

9.0 References 42

List of Tables

Table 1: Values for critical shear stress (van Rijn, 2007; Deltares, 2013). 13

Table 2: Regime coefficients for channels with sandy beds (after Lacey, 1930). 19

List of Figures

Figure 1: Conceptual compartment model of open water, marsh, and upland exchanges of water, salinity, temperature, sediment, and nutrients. 4

Figure 2: Intra- and intercompartment exchanges of water, salinity, temperature, sediment, and nutrients (plan view). 5

Figure 3: Settling velocity for sand particles for various diameters and Reynolds numbers. 8

Figure 4: Salinity effect on zone interface settling. 9

Figure 5: Salinity adjustment to settling velocity for flocculated particles used in Delft3D. 10

Figure 6: Dynamics of settling velocities, Ws, of flocculated particles as a function of the suspended fines concentration. 11

Figure 7: Settling velocities for Lake Okeechobee, as a function of particulate concentration. 11

Figure 8: Comparison of wave heights from USACE engineers (1984) and Young and Verhagen. 16

Figure 9: Example of a subdelta in the Lower Mississippi River showing bifurcations. 20

Figure 10: Stencil for delta building grid. 20

Figure 11: Open water-marsh exchange process.. 25

Figure 12: Decay of turbulent kinetic energy as a function of stem density (left) and setback (right) from the marsh edge. 27

Figure 13: Velocity profiles and sedimentation in salt marshes. 28

Figure 14: Definition of two-zone marsh. 28

Figure 15: Some factors affecting the distribution of marsh edge erosional material. 32

Figure 16: Flowchart for the hydrology subroutine of the ICM. 33

Figure 17: Flowchart for open water sediment processes. 33

Figure 18: Flowchart for marsh processes. 34

Figure 19: Annual corrections of open water area and accumulation for marsh edge retreat. 35

Figure 20: Integration of wave model with open water sedimentation. 35

Figure 21: Two zone treatment of marsh accumulation. 36

Figure 22: Suspended sediment response to a wind blowing for 24 hours in the southeast cell of Lake Pontchartrain.....37

Figure 23: Test for sand accumulation at a diversion.....37

Figure 24: Sand accumulation rate for a pulsed diversion before land-building.....38

Figure 25: Sand accumulation rate for a pulsed diversion after land-building. 38

Figure 26: Marsh stage response to tidal forcing in the open water; testing the Kadlec-Knight equation.. 39

Figure 27: Suspended sediment response to tidal flooding of the near edge marsh: testing the two-zone marsh concept......39

Figure 28: Suspended sediment response to tidal flooding of the interior marsh: testing the two-zone marsh concept.. 40

Figure 29: Suspended sediment response as cumulative accumulation to tidal flooding of the marsh: testing the two-zone marsh concept.....41

List of Abbreviations

CPRA	Coastal Protection and Restoration Authority
DEM	Digital Elevation Model
ECOMSED	Environmental Hydrodynamic and Sediment Transport
EwE	Ecopath with Ecosim
HSI	Habitat Suitability Index
ICM	Integrated Compartment Model
TKE	Turbulent Kinetic Energy
TSS	Total Suspended Sediment
USACE	United States Army Corps of Engineers
WASP	Water Quality Analysis Simulation Program
BIMODE	Barrier Island Model Development

1.0 Introduction

The objective of the sediment distribution and morphology effort was to investigate and, where possible, improve the sediment distribution processes that were used in the 2012 Coastal Master Plan eco-hydrology and wetland morphology models for incorporation into an Integrated Compartment Model (ICM), as described in the 2017 Coastal Master Plan Model Improvement Plan (CPRA, 2013) and Attachment C3-22: ICM Development.

The sediment distribution and morphology processes described in this report are incorporated into the ICM. Compartments within the ICM refer to hydrologic units consisting of open water, marsh and upland areas; the open water areas and the marsh areas are connected by conveyance links. The ICM consists of the following coupled subroutines: hydrology, morphology, vegetation, and barrier islands. The hydrology subroutine computes the hydrology, hydraulics, sediment transport, water temperature, salinity, sediment concentrations/accretion, and nutrients within compartments. The morphology subroutine computes land loss and land building and provides the digital elevation model (DEM) on which the hydrology compartments are based. The vegetation subroutine determines the marsh type, the vegetation type, habitat, etc. The hydrology subroutine has a relatively small time step of the order of 30 seconds and a large spatial scale of the order of a few square kilometers; this subroutine provides stage, salinity, water temperature, and sediment accretion to the other subroutines at intervals of one day to several years. At one-year intervals the morphology subroutine provides an updated DEM that is used by the hydrology subroutine to assign land area, open water area, and elevations to the hydrology compartments. The hydrology subroutine is subject to offshore boundary conditions on stage, salinity, water temperature, sediment concentration, and nutrient concentrations.

The ICM includes several improvements over the suite of models used to support the 2012 Coastal Master Plan, such as: additional processes in the hydrology, vegetation, wetland and barrier island morphology subroutines, increased spatial resolution, and integration of previously disparate models into a single modeling framework. The ICM also includes habitat suitability indices (HSIs) to predict broad spatial patterns of habitat change (refer to Attachments C3-6 through C3-19), and it provides input to a dynamic fish and shellfish community model which predicts potential changes in fishery resources (refer to Attachment C3-20: Ecopath with Ecosim (EwE)). The ICM can be used to estimate the individual and cumulative effects of restoration and protection projects on the landscape, including a general estimate of water levels associated with flooding.

The model domain was discretized into compartments. The general principle was to define compartments based on hydrologic units or sub-units. The boundaries of the compartments were manually imposed starting with a habitat map, and then manually adjusting the compartments to account for drainage patterns. Large open water areas were sub-divided to provide better resolution. The same was done for deltas and potential delta building areas.

The 2012 eco-hydrology model (Meselhe et al., 2013) is a compartment model that included open water, marsh, and upland areas. The model is classified as a link-node model in which the process computations are completed in the nodes, and the links are used to transfer quantities from node to node. The state variables were water levels, salinity, sediment concentrations, flow between nodes, water temperature, and nutrients. The sediment component of this model addressed two classes of material: inorganic fines (e.g., silt and clay) and sand. The fine sediment in the bed of the open water cell, or node, was subject to resuspension based on the excess bed shear relative to the critical bed shear; the bed shear was assumed to be proportional to wind speed squared, while the critical bed shear was related to a critical wind

speed squared. The critical wind speed was determined through the calibration procedure. The Krone (1962, 1966) formula was used for the deposition rate and the depositional velocity was determined by calibration. In open water, the net inorganic bed accumulation rate was the difference between the resuspension rate and the deposition rate. The transfer of sediment from the open water to the marsh occurred when the open water stage exceeded the marsh elevation; it was assumed that the flow into the marsh was sufficient to maintain the same stage in the marsh as in the open water. The flooding flow into the marsh is assumed to carry sediment at the same concentration as in the open water, but the ebbing flow is assumed to carry sediment at the concentrations in the water over the marsh; these sediment concentrations are reduced relative to the open water due to the sediment deposition in the marsh. Under non-hurricane conditions, only sediment deposition was considered in the marsh (i.e., no resuspension was considered). The sand class was deposited in the open water until the cell reached a limiting condition for bypassing. In some cases, a correction was required at the 25-year period to reset the flow and sediment distribution to simulate the delta building process.

The 2012 wetland morphology model used the compartmental mineral accumulation rates generated in the eco-hydrology model, along with biomass correlations, subsidence, and soil bulk density to convert the mineral accumulation rates into a revised DEM of the coastal landscape. The new DEM was used to update the marsh and open water elevations. These changes, in turn, were used to update the marsh and open water areas in the compartments of the eco-hydrology model on a 25-year interval. This process has been improved for the 2017 ICM by computing mineral accumulation rates in the open water, the near edge zone of the marsh, the interior of the marsh, and more frequent revisions of the land-water characteristics of each compartment. A separate report (Attachment C3-2: Marsh Edge Erosion) describes the marsh edge erosion procedure that is utilized in the morphology subroutine to generate the new marsh edge length and the change in marsh/open water areas. Two types of marsh sedimentation processes are considered: a) non-hurricane sediment transfer and b) hurricane accretion. The sediment distribution processes related to hurricanes includes some limits on sediment resuspension and bed erosion in open water areas.

The fate of mineral sediment in the coastal area involves sediment sources, sediment transport within the coastal area, sediment transfer to and from the marsh areas, and sedimentation processes within the marsh areas. There are distinct temporal and spatial differences related to tropical and frontal systems that the coastal sediment distribution must account for.

The sediment distribution processes within the hydrology subroutine focus on the interior coastal waters and marshes; marsh edge erosion processes are also considered in the hydrology subroutine, and the BIMODE subroutine focuses on the barrier islands (Attachment C3-4: Barrier Island Model Development). The purpose of this report is to summarize the findings of the literature search on coastal sediment distribution (Attachment C3-1.1: Sediment Distribution Supporting Information) and to describe the approach used to include sediment distribution processes in the hydrology subroutine of the ICM.

The areas of emphasis in this report are:

- Sediment processes in the open water areas
- Sediment transfer processes between the open water and the marsh areas
- Sediment processes in the marsh areas
- The effects of hurricanes (also referred to as tropical storms) on the sedimentation processes
- Available modeling frameworks for the simulation of coastal sediment distribution and morphology as a part of an integrated compartment model

The sediment distribution processes described in this report track the mineral sediments in the marshes and open waters of the coastal area. They are based in part on an extensive literature review (Attachment C3-1.1: Sediment Distribution Supporting Information). The modeling requirements are:

- Mass balance approach as per the 2012 Coastal Master Plan - Appendix D, CPRA 2012 and Meselhe et al., 2013
- Critical shear stresses for deposition and erosion
- Material class sizes to include sand, silt, colloidal, and flocculated clay
- Open water bed shear based resuspension process
- Channel bed shear model following van Rijn (1984, 2000, 2013)
- Marsh deposition model excluding hurricanes
- Net marsh accumulation due to hurricanes
- Open water deposition
- Marsh edge erosion and distribution of sediment
- Change in open water-to-land ratio
- Separate accumulation models for marsh and open water

Figure 1 shows the arrangement of compartments for the hydrology subroutine, which incorporates the sediment distribution computations (for details, see the 2012 Coastal Master Plan Appendix D; CPRA, 2012). Each compartment can have up to three subcompartments, namely open water, marsh, and upland. Figure 2 illustrates the assumed open water to marsh exchange; the marsh subcompartments are linked to the adjacent open water subcompartment with a "marsh" number corresponding to the open water number. There are no links from the marsh to another marsh subcomponent. If no marsh exists, the exchange is set to zero. In large marsh areas, the open water compartments and bayous are collected to form the open water cell so that flow between marshes can occur. In the 2012 Coastal Master Plan, the wetland morphology model provided data for the development of the initial DEM that was used to set up the areas and elevations of the marsh and the open water in the eco-hydrology model. Subsequently, the sediment accumulation was computed within the eco-hydrology model and used to revise the wetland morphology model to update the DEM. In the 2017 ICM, the sediment accumulation in the open water and marshes will be computed in the hydrology subroutine; the marsh accumulation will be computed in two zones: near edge and interior. These accumulation rates will be used in the morphology subroutine to update the DEM.

In the 2012 eco-hydrology model, a mass balance approach was applied to the sediments in both the open water and marsh subcompartments. In addition, there were upland subcompartments that are not subject to the normal tidal flood-ebb cycle; these were included to provide runoff related precipitation-evapotranspiration inputs. Equation 1 gives the general form of the mass balance that was used for each sediment class.

$$\frac{\partial C_{k,j}}{\partial t} = -\frac{C_{k,j}\eta'_j}{y_j} + \frac{\sum_i \sum_{trib} \sum_{div} \left[C_{k,j,i,trib,div} Q_{i,trib,div}\right]}{y_j A_{s,j}} + \frac{f_{dis} \sum_i \lambda_i \frac{A_i}{L_i} (C_{k,j} - C_{k,nb})}{y_j A_{s,j}} + \frac{\sum_l S_{r,k,j,l}}{y_j A_{s,j}} \qquad (1)$$

where: k = species (sediment class);
j = number of subcompartment;
i = number of link;
trib = tributary;

div	=	diversion;
nb	=	subscript referring to the neighboring subcompartment;
dis	=	dispersivity;
r	=	source-sink;
s	=	surface;
l	=	source/sink index;
$C_{k,j}$	=	concentration of constituent k in subcompartment j;
Q	=	water discharge;
$A_{s,j}$	=	subcompartment water surface area;
$\eta_{,}$	=	subcompartment water elevation;
η'	=	rate of change of elevation = $d\eta/dt$;
$S_{r,k,j,l}$	=	subcompartment sources/sink;
$y_{,j}$	=	subcompartment water depth;
t	=	time;
f_{dis}	=	calibration factor;
λ	=	diffusivity in link i (function of cross-sectional area);
L_i	=	effective link length;
$\frac{\partial C}{\partial t}$	=	rate of change of concentration in a cell.

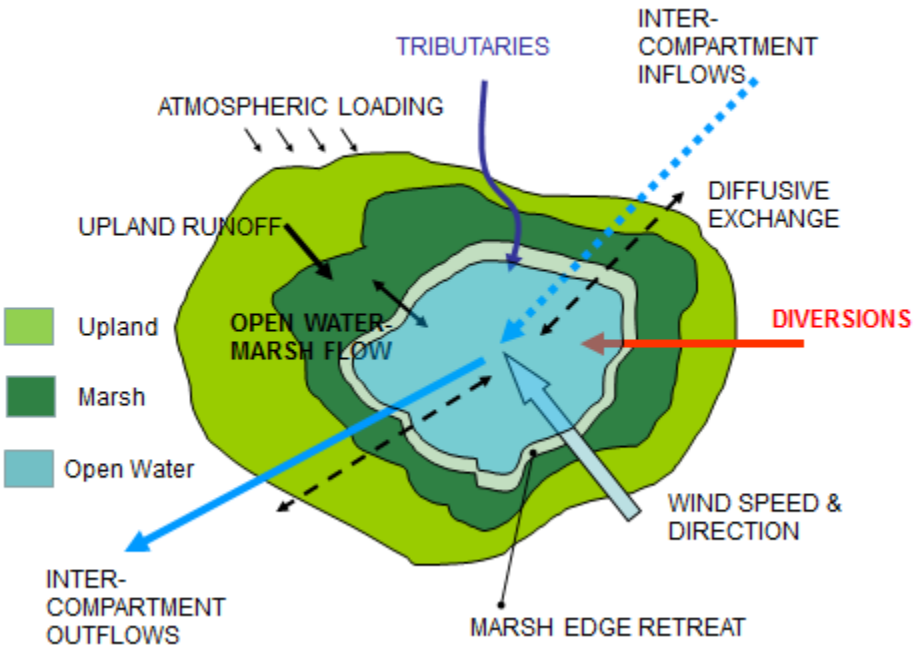

Figure 1: Conceptual compartment model of open water, marsh, and upland exchanges of water, salinity, temperature, sediment, and nutrients.

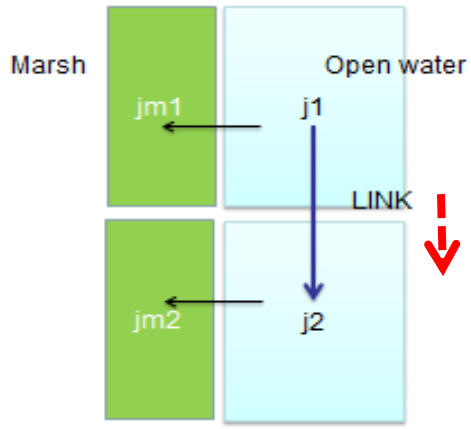

Figure 2: Intra- and intercompartment exchanges of water, salinity, temperature, sediment, and nutrients (plan view).
Note: the marsh numbers are referenced one-to-one to the adjacent open water numbers. The red dashed arrow indicates an overland or marsh to marsh link.

The same water balance that was used in 2012 Coastal Master Plan modeling effort will be used for 2017. The flow into the marsh (flooding) is computed by the difference in water level between the open water and the marsh; the return (ebb) flow is computed based on the difference in the marsh water level and the open water level. A level marsh flooding surface is assumed. The open water node is connected to the neighboring open water nodes and to the adjacent marsh node; in addition, the marsh node cannot directly pass flow to another marsh node via an overland link. If a marsh does not adjoin the open water, there is no marsh flow exchange for this compartment. The specific treatment for the type of vegetation in the marshes was not implemented in this version of the subroutine because of the large uncertainty in the suggested values of '*a*' (Kadlec & Knight, 1996). The flow (m^3d^{-1}) into and out of the marsh is computed by the Kadlec and Knight (1996) formula:

$$Q_{marsh} = (a \times 10^7) W (H)^3 \left(\frac{\eta_{OW} - \eta_M}{L}\right) \quad (2)$$

where:
- a = calibration coefficient ($m^{-1}d^{-1}$); depends on the marsh type; however, a global value of 'a' is used in the present version of the ICM;
- W = width of the flow path (m; e.g., length of marsh edge);
- H = marsh water depth (m) constrained by a nonzero minimum value;
- η_{OW} = stage elevation (m) in the open water (replace E with η);
- η_M = stage elevation (m) in the marsh (replace E with η);
- L = distance (m) between the stage locations, approximated by the near edge zone.

A positive flow indicates flow into the marsh, and a negative flow indicates flow leaving the marsh.

2.0 Open Water Sediment Distribution Processes

For each open water model compartment, a mass balance is calculated. Inflows to each compartment contain a calculated value for total suspended sediment (TSS), which is partitioned into four inorganic classes: sand, silt, flocculated, and colloidal clay. Extensive literature exists on the role of wind on resuspension of sediment in shallow water; for example,

Anderson (1972, 1970); Grant (1979); Glenn (1987); Bacon (1994); Biscaye (1988); Blom and Aalderink (1998); Booth et al. (2000); Chang et al. (2001); Georgiou et al. (2007); Roblin (2007); McCorquodale et al. (2010); Meselhe et al. (2013); and Erm et al. (2011) have contributed to existing literature on the role of wind. The following discussion of the literature provides the mathematical equations for open water sediment distribution processes for the ICM hydrology subroutine.

The deposition pattern of the sediment at a diversion is expected to follow a fan or delta formation (Coleman, 1988). Coleman's work showed subdeltas (e.g., on the lower Mississippi River) went through an advancing stage for about 50 years until they reached a limiting radius of about 20 km; thereafter, they began to erode, possibly because the energy gradient was insufficient to sustain growth. The pattern of links and nodes that distribute flow from the receiving point of a diversion should mimic the bifurcation process in these subdeltas. Coleman's (1988) research can be used to estimate the ultimate radius of the delta fan. This appears to be a function of the available energy head and the required shear stress to move the bed load. For example, Cubit's Gap developed its maximum radius of about 16 km in about 70 years, with a maximum energy head of approximately 0.8 m, which gives an energy gradient of 1/20,000 or a maximum shear stress of approximately 3 Pa. The critical shear stress for fine sand is about 0.2 Pa or a van Rijn (1984) dimensionless excess shear stress T of approximately 16. Esposito et al. (2013) reported that "river mouth bar" formation in the subdelta of Cubit's Gap controlled the bifurcations in the delta. Yocum et al. (2013) studied Brant's Splay and related the bifurcation to the "river mouth bar" interval, L_{RMB}.

$$L_{RMB} = K_L d \left[\frac{U^2}{(S_s - 1) g D_{50}} \right]^{0.2278} \quad (3)$$

where:
- d = depth;
- g = acceleration due to gravity;
- S_s = Specific gravity of the sediment;
- D_{50} = median grain size;
- U = channel velocity before bifurcation;
- K_L = 70.

Equation 3 indicates a first order bifurcation at about 1 km for subdeltas such as Cubit's Gap and Baptiste Collette. L_{RMB} can be used as a length scale based on channel geometry, channel velocity, and sediment size for designing a stencil for land building deltas, which will be discussed in more detail in Section 2.3 – Routing of Suspended Sediments. The channel geometry can be related to the sediment size and dominant flow by regime relationships such as those of Lacey (1930). The smallest compartment sizes in the current version of the model grid are of the order of 1 km^2 which is consistent with the mouth bar spacing.

2.1 Deposition of Suspended Sediments

A sediment deposition rate (m/s) for each open water compartment is calculated from the settling velocity of suspended sediment in the water column. Since the compartments are considered fully mixed, the TSS concentration is assumed constant throughout the water column. In the 2012 Coastal Master Plan, a single settling velocity was calculated as a function of TSS concentration. However, the updated sediment deposition subroutine partitions the TSS into sand, silt, flocculated clay, and colloidal clay which requires separate settling velocities to be calculated for each sediment class. The settling velocity, w_s, for each of these classes is calculated from Stokes' law (King & Galvin, 2002).

$$w_s = \sqrt{\frac{4gD_{50}}{3C_D}\left(\frac{\rho_s}{\rho_w} - 1\right)} \quad (4)$$

where: D_{50} = median diameter of particles within the sediment class (m);
ρ_s = particle density (kg/m^3);
ρ_w = density of the water, which is a function of water temperature and salinity (kg/m^3);
g = acceleration due to gravity (ms^{-2});
C_D = dimensionless drag coefficient.

Representative particle diameters and densities and/or settling velocities are determined for each sediment class from existing calibration datasets. However, the dimensionless drag coefficient (C_D) is a function of the Reynolds number which is a function of the settling velocity. Rather than implementing an iterative solution, the drag coefficient for small particles (silt and clay) with slow settling velocities (Reynolds number < 0.5) is estimated by:

$$C_D = \frac{24\nu}{w_s D_{50}} \quad (5)$$

where ν is the kinematic viscosity (King & Galvin, 2002). Substituting this into Equation 4 results in a settling velocity for silt and clay particles.

$$w_s = \frac{g{D_{50}}^2}{18\upsilon}\left(\frac{\rho_s}{\rho_w} - 1\right) \quad (6)$$

While Equation 6 can be used for determining settling velocities for silt and clay, it is not applicable for sand particles, which typically have a Reynolds number greater than 0.5. As reproduced from the Coastal Engineering Manual (U.S. Army Corps of Engineers [USACE], 2002), Figure 3 can be used to estimate settling velocities for sand particles for a given D_{50}. Equation 7 is a useful closed form solution of Equation 4 (Ackers & White, 1975; White et al., 1978) for the settling velocity; this approach was selected because it gives a non-iterative solution and avoids need for the chart.

$$w_s = F\sqrt{(S_s - 1)d_g g} \quad (7a)$$

where

$$F = \sqrt{\frac{36}{{D_r}^3} + \frac{2}{3}} - \sqrt{\frac{36}{{D_r}^3}} \quad (7b)$$

and

$$D_r = d_g\sqrt{\frac{g(S_s - 1)}{\upsilon^2}} \quad (7c)$$

where: d_g = grain size (m);
S_s = specific gravity of the grain;
υ = kinematic viscosity (m^2/s);
g = acceleration due to gravity (ms^{-2});
F = velocity factor;
D_r = non-dimensional particle diameter.

White et al. (1978) also provided an equation for kinematic viscosity (m^2/s) as a function of water temperature, T (◦ C):

$$\upsilon = \frac{1.79 \times 10^{-6}}{1 + 0.03369T + 0.000221T^2} \quad (7d)$$

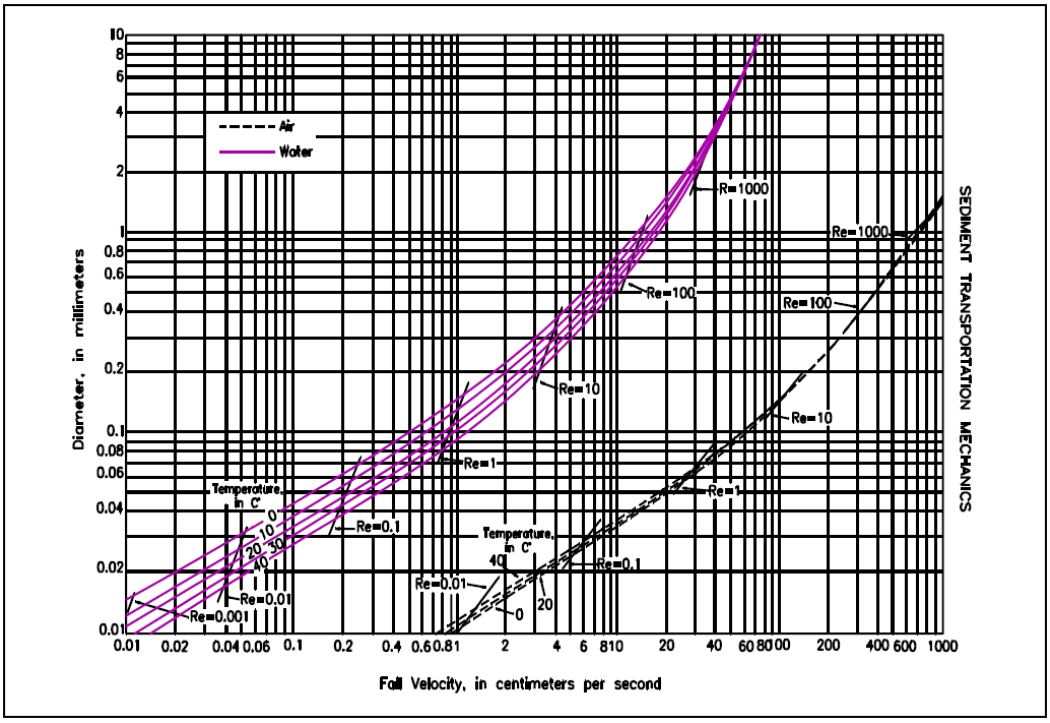

Figure 3: Settling velocity for sand particles for various diameters and Reynolds numbers (as presented in King & Galvin, 2002).

2.1.1 Flocculation

While sand, silt, and nonflocculated clay particles will settle out of the water column at the rates calculated above, the settling velocity for a portion of the clay particles must be adjusted to take flocculation into account. Flocculation is a complex process with many driving factors, including mineral properties, biological properties, sediment concentration, salinity concentration, and turbulence (Deltares, 2013; Mikeš & Manning, 2010; McAnally et al., 2007; Mehta et al., 1991, Kotylar et al., 1996). There is insufficient data to explicitly include some of these, such as biological factors; however, two of the most important (i.e., sediment and salinity concentrations) are accounted for in the hydrology subroutine. First, the fraction of clay particles which form floc, P_{floc}, are estimated as a function of the salinity concentration.

$$P_{floc} = \begin{cases} \frac{C_{sal}}{C_{sal,max}} P_{floc,max} & C_{sal} < C_{sal,max} \\ P_{floc,max} & C_{sal} \geq C_{sal,max} \end{cases} \quad (8)$$

where: $P_{floc,max}$ = upper limit to the fraction able to flocculate;
C_{sal} = salinity concentration;
$C_{sal,max}$ = salinity threshold.

Salinity concentrations above this threshold result in no increase to flocculation; a threshold of 5 ppt was used in the 2012 Coastal Master Plan, which was based on Kotylar et al. (1996) and utilized in Lake Pontchartrain modeling efforts. P_{floc} is treated as a calibration parameter, with an initial estimated value of 0.5, indicating that half of the suspended clay particles are available for flocculation. Figure 4 shows that the settling rate has a rapid response to salinity up to approximately 5 ppt; the settling interface refers to the interface that develops between the clarified liquid and the sediment laden liquid in the case of zone or hindered settling. A linear relationship presented between P_{floc} and C_{sal} was selected for Equation 8, due to the nearly linear equation used in the Delft3D-FLOW model to adjust flocculated settling velocities as a function of salinity (Figure 5; Deltares, 2013). This approximation simplifies the code, but the Delft3D curve could be used in future efforts if further testing indicates that the solution is significantly changed by this assumption.

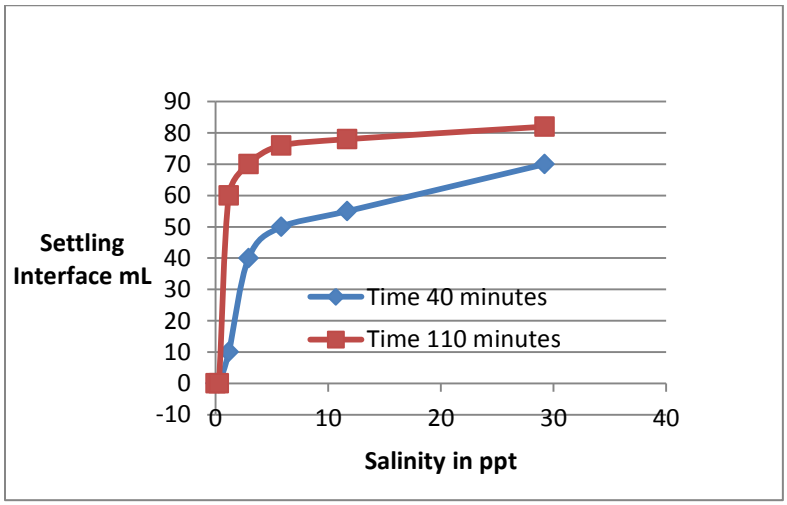

Figure 4: Salinity effect on zone interface settling (after Kotylar et al., 1996).

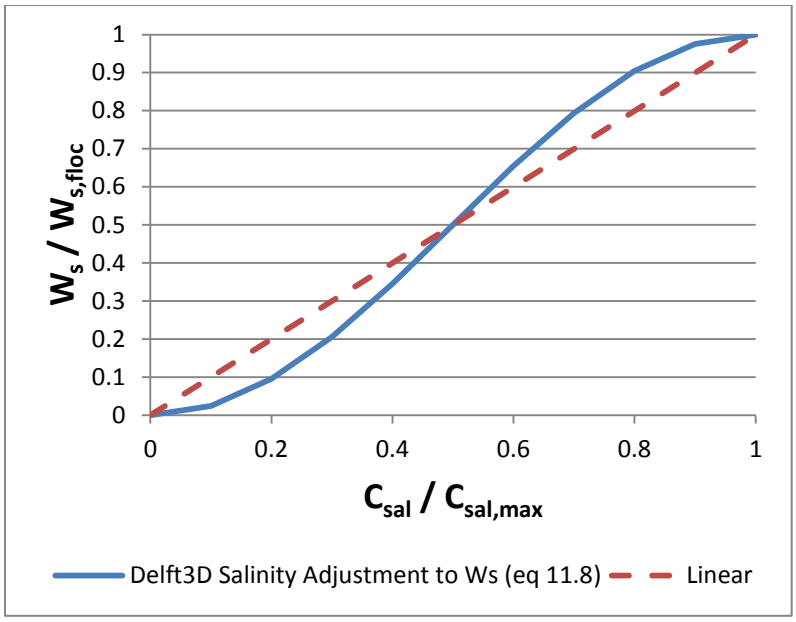

Figure 5: Salinity adjustment to settling velocity for flocculated particles used in Delft3D (after Deltares, 2013).

Once the portion of flocculated clay sediments is calculated from the salinity concentration, a settling velocity is calculated for these flocculated particles. While the settling velocity of flocculated particles will initially increase with an increase in the concentration of suspended clay, at a certain threshold, the settling velocities will decrease (McAnally et al., 2007).

The dynamics of flocculated settling velocities, as depicted in Figure 6, are incorporated into the sediment distribution processes in the hydrology subroutine by calculating settling velocities for flocculated clay particles, $w_{s,floc}$, as:

$$w_{s,floc} = \begin{cases} w_s & C_{clay} < C_1 \\ a\dfrac{{C_{clay}}^n}{\left({C_{clay}}^2 + b^2\right)^m} & C_1 < C_{clay} < C_3 \\ negligible & C_3 < C_{clay} \end{cases} \quad (9)$$

Where: C_{clay} = total suspended clay concentration (kg/m^3);
w_s = settling velocity of nonflocculated clay particle (Equation 6);
a = 33.38;
b = 2.537;
n = 1.83;
m = 1.89;
C_1 = 0.1 kg/m^3;
C_3 = 4.38 kg/m^3.

These values were chosen from a study of flocculated sediments from Lake Okeechobee, as shown in Figure 7 (Mehta et al., 1991). Lake Okeechobee is a small shallow lake which is similar in

size and depth to several water bodies in coastal Louisiana (e.g., lakes in the Chenier Plain, Lake Pontchartrain, Lake Maurepas, Lake Borgne, and Lake Salvador).

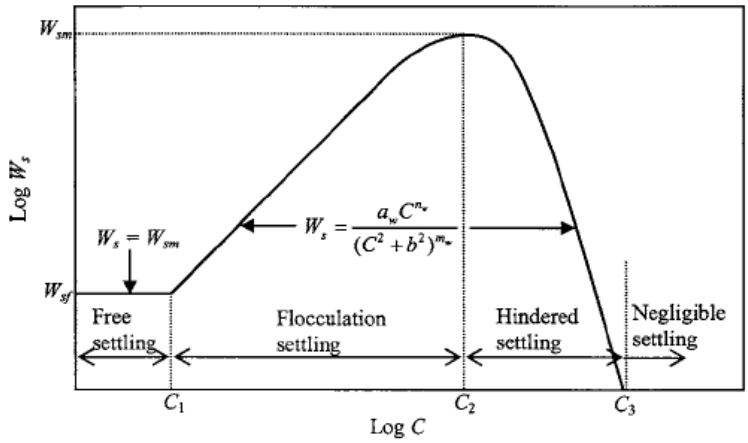

Figure 6: Dynamics of settling velocities, Ws, of flocculated particles as a function of the suspended fines concentration (from McAnally et al., 2007).

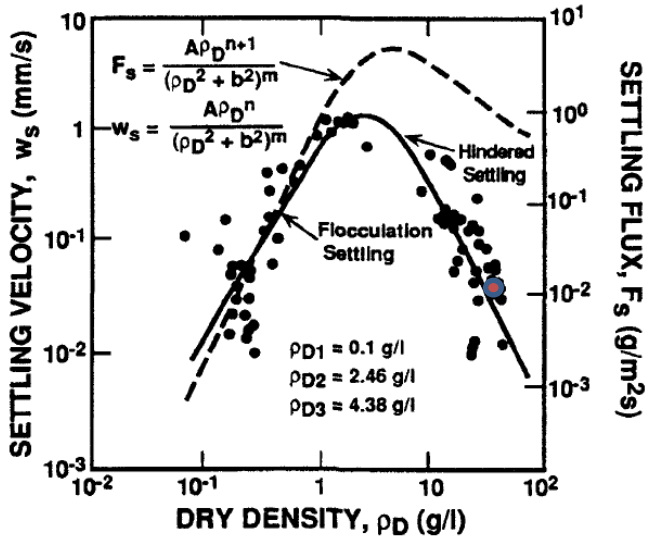

Figure 7: Settling velocities for Lake Okeechobee, as a function of particulate concentration. "Dry density"= particle dry mass/suspension volume (from Mehta et al., 1991). The Lake Pontchartrain silt/floc settling velocity is indicated by the red circle.

The coefficients in Equation 9 are presented as initial values. Possible ranges are: C_1 = 0.1 – 0.3 kg/m^3; C_3 = 2 – 5 kg/m^3 (McAnally et al., 2007).

The flocculent settling was found to be approximately 8 m/day (approximately 0.1 mm/s as shown in Figure 7) in Lake Pontchartrain at a suspended solids concentration of 40 to 300 mg/L and salinity of the order of 5 ppt (Roblin, 2010; Haralampides, 2000); this value will be used as an initial value but the final value will be established by calibration based on observed suspended solids data (see Attachment C3-23: ICM Calibration, Validation and Performance Assessment).

Finally, it is necessary to convert the flocculent settling velocity to the depositional velocity (V_d) of cohesive sediment which is related to the settling velocity by the Krone (1962, 1966, 1986) formula.

$$v_{d,k} = w_{s,k}\left(1 - \frac{\tau_{bed}}{\tau_{d,k}}\right) \quad (10)$$

where: $w_{s,k}$ = settling velocity for class k;
k = subscript indicating the class of cohesive sediment;
τ_{bed} = bed shear stress;
$\tau_{d,k}$ = critical shear stress for initiation of deposition of class k.

Equation 10 is applicable for $\tau_{bed} < \tau_{d,k}$. For this modeling effort, the depositional critical shear was equated to the erosional critical shear since there is insufficient field data to distinguish between these parameters. If the critical shear for deposition is greater than the critical shear for resuspension, there will be an over-estimation of the deposition rate; however, since the quiescent periods between storms allows the completion of most flocculent deposition, there should not be a large error due to this assumption. The Krone formula partially accounts for near bed turbulence by introducing the shear stress at the bed. Turbulence is important in flocculation; however, it is assumed that this is accounted for during calibration.

2.2 Resuspension

In addition to deposition, sediment resuspension is calculated in the 2017 ICM. Due to the inclusion of sediment classes, two resuspension approaches are included: one for cohesive particles (e.g., silt, flocculated clay, and colloidal clay) and one for noncohesive particles (e.g., sand). The effect of the root zone in the marshes and biofilms or exocellular polymers have not been considered in this modeling effort.

2.2.1 Resuspension of Silt and Clay Particles

Resuspension of silt and clay particles is estimated from an equation similar to one used in the 2012 Coastal Master Plan eco-hydrology modeling effort (CPRA, 2012; Meselhe et al., 2013); however, bed shear stresses are calculated from wave prediction equations and the currents, as opposed to using wind statistics as a proxy for bed shear. Sediment resuspension, E_{res}, is calculated for silt and clay as:

$$E_{res} = \frac{a_c}{T_{res}T_{con}{}^{m}}\left(\frac{\tau_{bed}}{\tau_{cr}} - 1\right)^{n} \quad (11)$$

where: a_c = function of the bed properties (to be determined by calibration);
T_{res} = response time of the bed (typically assumed to be equal to 1 hour);
T_{con} = time since deposition of sediment;
τ_{bed} = bed shear stress;
τ_{cr} = critical shear stress which will result in resuspension for the sediment class;
m = calibration constant;
n = calibration constant.

Currently, there are insufficient data on the surficial sediment in the coastal area to include all of the bed factors in the formulation for a_c. Therefore, the following coefficients have been lumped together into a single calibration parameter with the assumption that n equals 1: a_c, T_{res}, T_{con}, and m. This approach has been used for cohesive sediment resuspension in widely used hydrodynamic models: Delft3D (Deltares, 2013) and Environmental Hydrodynamic and Sediment Transport (ECOMSED; HydroQual, 2002). The critical shear stress for resuspension of silt and clay is assumed to be the same.

Typical values for critical shear stresses for various sediment classes are provided in Table 1; bed shear stress is calculated from the Young and Verhagen wave model and linear wave theory, as discussed in a later section. Jerolleman (2014) used the Lick Shaker Test (Sheng & Lick, 1979; Haralampides, 2000) to measure the critical shear stress for erosion of cohesive marsh bed sediments as a function of consolidation time. The results show that the critical shear stress increases nearly linearly from approximately 0.02 Pa to 0.1 Pa in six days. Since the inter-storm (extra-tropical or frontal systems) period is roughly six days, the critical shear stress of 0.1 Pa in Table 1 appears to be justified.

Table 1: Values for critical shear stress (van Rijn, 2007; Deltares, 2013).

Particle size	Critical shear, τ_{cr}	Notes
6 µm	0.25 N/m^2	quartz particles in cohesive beds with bulk densities of 1,600-1,900 kg/m^3 (Roberts et al., 1998)
50 µm	0.08 N/m^2	quartz particles (Roberts et al., 1998)
8 – 62 µm	0.1 N/m^2	weakly consolidated, fine sediments
> 200 µm	0.2 – 0.4 N/m^2	Sand

2.2.2 Bed Shear Stress

A critical component of the sediment distribution calculations described above is the bed shear stress (HydroQual, 2002), which is calculated from:

$$\tau_{bed} = C_f \rho_w {U_{bed}}^2 \quad (12)$$

where: C_f = friction coefficient = constant in the range 0.001 to 0.003 (f refers to friction)
U_{bed} = velocity near the bed

The value of C_f will be fine-tuned in the final calibration process (see Attachment C3-23: ICM Calibration and Validation); however, a value of 0.0025 corresponds to a Manning's n of 0.018. Velocity at the bed, U_{bed}, is calculated as follows:

$$U_{bed} = \mathrm{U} + U_{tide} + U_w + U_{orb} \quad (13)$$

where: U = velocity due to flow discharge from tributaries and diversions;

U_{tide} = velocities induced by tide;
U_w = wind driven current;
U_{orb} = orbital velocity at the bed due to waves.

The velocity in the compartment due to discharges such as diversions and tributaries and tide, (U+U_{tide}), are determined from the flows in and out of the open water compartment:

$$U + U_{tide} = \left\{\sum |Q_{in}| + \sum |Q_{out}|\right\}/2A_x \quad (14)$$

where: Ax = the effective cross-section of the open water cell (width x depth in m^2);
Qin = the inflow to the open water (m^3/s);
Qout = the outflow for the open water cell(m^3/s).

The cell width is assigned in the cell attributes and the depth is computed in the hydrodynamic simulation.

The wind induced circulation currents (Ekman, 1905; Keulegan, 1951; Rossby and Montgomery, 1936) are estimated from wind speed, U_{10}, by:

$$U_w = k_a U_{10} \quad (15)$$

where: k_a is in the range 0.023 to 0.032;
U_{10} is the wind speed at 10 m above the water surface.

The wave induced orbital velocity at the bed, U_{orb}, is estimated from linear wave theory:

$$U_{orb} = \frac{gH_s T \cosh\left(\frac{2\pi z}{L}\right)\cos\theta}{2L\cosh\left(\frac{2\pi d}{L}\right)} \quad (16)$$

The orbital velocity is calculated at the bed; therefore, the height above the bed (z) in Equation 16, equals zero. The above expression is calculated for a maximum orbital velocity that occurs at a wave phase of θ=0, resulting in Equation 16, reducing to Equation 17 (Demirbilek & Vincent, 2002).

$$U_{orb} = \frac{gH_s T}{2L\cosh\left(\frac{2\pi d}{L}\right)} \quad (17)$$

where: g = gravitational acceleration (m/s^2);
H_s = significant wave height (m);
T = wave period (s);
L = wavelength (m);
d = water depth (m).

Wavelength can be iteratively solved from depth and wave period (Equation 18). However, a reasonably accurate (±10%), non-iterative approximation corrected for wavelength (Equation 19) can be used for simplicity (Demirbilek & Vincent, 2002).

$$L = \frac{gT^2}{2\pi}\tanh\left(\frac{2\pi d}{L}\right) \quad (18)$$

$$L \approx L_o\sqrt{\tanh\left(\frac{2\pi d}{L_o}\right)} \quad (19)$$

$$L_o = \frac{gT^2}{2\pi} \quad (20)$$

where: L_o = deep water wave length.

Equations 16 through 20 require three input variables: wave period, *T*, water depth, *d*, and significant wave height, H_s; only one of which, *d*, was calculated in the 2012 Coastal Master Plan open water compartments. Therefore, the Young and Verhagen (1996) wave model has been incorporated into the open water calculations to calculate the final two parameters needed for bed shear calculations, *T* and H_s.

From fitting established wave spectrum equations to observed datasets, Young and Verhagen (1996) developed empirical relationships for wave energy, *E* (m^2), and frequency, *f* (hz), which is the reciprocal of wave period, *T*.

$$E_{wave} = E_{wave\ lim}\left\{\tanh A_1 \tanh\left(\frac{B_1}{\tanh A_1}\right)\right\}^n \left(\frac{{U_{10}}^2}{g}\right)^2 \quad (21)$$

$$\frac{1}{T} = f = f_{lim}\left\{\tanh A_2 \tanh\left(\frac{B_2}{\tanh A_2}\right)\right\}^m \left(\frac{g}{U_{10}}\right) \quad (22)$$

$$A_1 = 0.292^{1/n}\left[d\frac{g}{{U_{10}}^2}\right]^{1.3/n} \quad (23)$$

$$B_1 = (4.396\times 10^{-5})^{1/n}\left[X\frac{g}{{U_{10}}^2}\right]^{1/n} \quad (24)$$

$$A_2 = 1.505^{1/m}\left[d\frac{g}{{U_{10}}^2}\right]^{-0.375/m} \quad (25)$$

$$B_2 = 16.391^{1/m}\left[X\frac{g}{{U_{10}}^2}\right]^{-0.27/m} \quad (26)$$

where: *d* = depth (m);
X = fetch (m);
f = wave frequency (hz);
U_{10} = wind speed at 10 meters (m/s);
$E_{wave\ lim}$= 0.00364;

f_{lim} = 0.133;
n = 1.74;
m = -0.37;
and all other variables are as previously defined.

Ongoing studies (Georgiou, 2013; Trosclair, 2013) in the Biloxi marsh indicate that coefficients originally proposed by Young and Verhagen for Equations 21 through 26 produce acceptable results for water bodies in the Gulf Coast region.

The wave period, T, is the reciprocal of wave frequency (Equation 22) and the significant wave height, H_s, can be estimated from Equations 21 and 27 (Demirbilek & Vincent, 2002; Young & Verhagen, 1996).

$$H_s = 3.8\sqrt{E_{wave}} \approx 4\sqrt{E_{wave}} \quad (27)$$

Filostrat (2014) compared the Young and Verhagen wave heights with the USACE Shore Protection Manual (USACE, 1984) and found that there was good agreement between these two methods for shallow water bodies as indicated by Figure 8. The reader is also referred to Dupuis (2013) for comparisons with observed wave data.

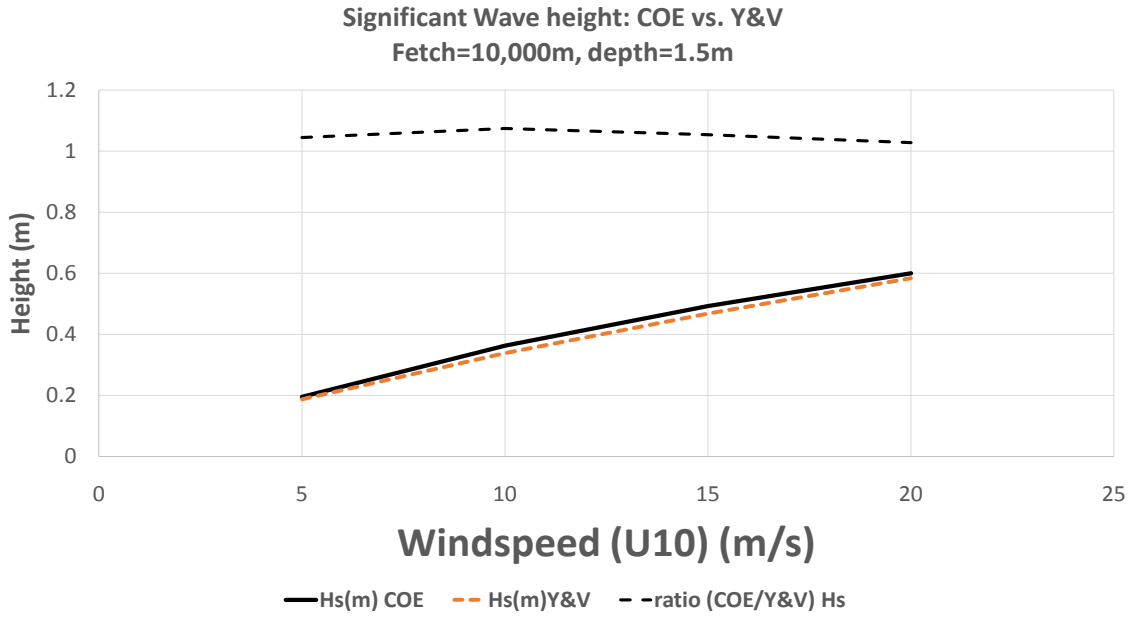

Figure 8: Comparison of wave heights from USACE engineers (1984) and Young and Verhagen (after Filostrat, 2014).

The Young and Verhagen (1996) wave model is applicable to fetch-limited wave conditions, a condition that requires that the wind speed being used in the above equations has been sustained for a long enough period to reach fetch-limited waves. A process outlined in the Coastal Engineering Manual (USACE, 2002) was followed to ensure that fetch-limited conditions were met. The duration that the wind speed should be sustained to reach these conditions is determined by:

$$t_{req} = 77.23 \frac{X^{0.67}}{{U_{10}}^{0.34} g^{0.33}} \quad (28)$$

If the averaging interval used in the wind data is less than this required duration, t_{req}, an equivalent fetch, X_{eq} must be calculated and substituted for fetch, *X*, in the Young and Verhagen equations (Equations 21 – 26; Resio et al., 2002). The equivalent fetch was calculated from the timestep used to average the wind record, t_{dur}, and wind velocity at 10 m above the surface, U_{10}.

$$X_{eq} = 5.23 \times 10^{-3} \sqrt{{t_{dur}}^3 g u_*} \tag{29}$$

$$u_* = U_{10} \sqrt{C_D} \tag{30}$$

$$C_D = 0.001(1.1 + 0.035 U_{10}) \tag{31}$$

The details for the incorporation of equations into the hydrology subroutine of the ICM are discussed in the final section of this report.

2.2.3 Resuspension of Sand Particles

Equation 11 is used to determine resuspension of clay and silt particles; however, a method developed by van Rijn (2007a) provides the mechanics for the resuspension of sand particles in channelized flow. To accommodate the sand transport equations, the open water can be treated as an equivalent channel. Sand particles are resuspended into the water column if the dimensionless shear stress, θ, is greater than the dimensionless critical shear stress which defines the initiation of motion for sand particles, θ_{cr}.

$$\vartheta_{cr} = \frac{\tau_{cr}}{(\rho_s - \rho_w) g D_{50}} \tag{32}$$

Typical values for critical shear stress, τ_{cr}, are provided in Table 1; all other variables are as previously defined. Empirical values for critical shear stress for initiation of motion of sand particles, θ_{cr}, have been developed by van Rijn (2007a) and others.

$$\vartheta_{cr} = \begin{cases} 0.115 {D_*}^{-0.5} & D_* < 4 \\ 0.14 {D_*}^{-0.64} & 4 \le D_* < 10 \end{cases} \tag{33}$$

$$D_* = D_{50} \left[\frac{g\left(\frac{\rho_s}{\rho_w} - 1\right)}{\upsilon^2} \right]^{1/3} \tag{34}$$

If θ, is calculated to be greater than θ_{cr}, the rate of sediment resuspension (in kg/s/m) can be calculated from Equations 35 through 40 (van Rijn, 2013).

$$q_s = \alpha_s \rho_s u D_{50} {M_e}^{2.4} {D_*}^{-0.6} \tag{35}$$

$$M_e = \frac{(u_e - u_{cr})}{\sqrt{gD_{50}\left(\frac{\rho_s}{\rho_w} - 1\right)}} \tag{36}$$

$$u_e = u + \gamma u_{orb} \tag{37}$$

$$u_{cr} = \left(\frac{u}{u + u_{orb}}\right) u_{cr,c} + \left(1 - \frac{u}{u + u_{orb}}\right) u_{cr,w} \tag{38}$$

$$u_{cr,c} = \begin{cases} 0.19{D_{50}}^{0.1} \log\left(\frac{12d}{3D_{90}}\right) & 0.1\ mm < D_{50} < 0.5\ mm \\ 8.5{D_{50}}^{0.6} \log\left(\frac{12d}{3D_{90}}\right) & 0.5\ mm < D_{50} < 2\ mm \end{cases} \tag{39}$$

$$u_{cr,w} = \begin{cases} 0.24\left[\left(\frac{\rho_s}{\rho_w} - 1\right) g\right]^{0.66} {D_{50}}^{0.33} T^{0.33} & 0.1\ mm < D_{50} < 0.5\ mm \\ 8.5\left[\left(\frac{\rho_s}{\rho_w} - 1\right) g\right]^{0.57} {D_{50}}^{0.43} T^{0.14} & 0.5\ mm < D_{50} < 2\ mm \end{cases} \tag{40}$$

where: u = depth-averaged velocity for each time-step considering all flow forcings (m/s);
α_s = coefficient ranging from 0.008 to 0.012;
γ = coefficient which is either 0.4 for irregular waves or 0.8 for regular waves;
D_{90} = 90th percentile particle diameter (m);
D_{50} = 50th percentile particle diameter (m);
T = wave period(s);
and all other variables are as previously defined.

2.3 Routing of Suspended Sediments

It should be noted that links are hydraulic conveyances that do not involve mass or water volume balance; these are handled by the hydrology compartments. In the 2012 Coastal Master Plan eco-hydrology model, there was a tendency for excessive sediment build-up in the compartments at the deltas and diversions. The reasons for this were: 1) the infrequent (25-year) updating of the land area within the cells, 2) the lack of a robust procedure for bypassing sand as the compartment filled up, and 3) the need for more resolution in areas of interest. This was overcome by readjusting the link capacities and bypassing sediment when the velocity in an open water area exceeded a certain value, using a penalty function that decreased the trap efficiency as the flow-through velocity approached a critical limit. To avoid excessive deposition, a significant refinement to the spatial resolution of the compartments was necessary (particularly those closest to existing and proposed diversion outlets), as well as a robust flow and sediment distribution algorithm.

The links are generally based on actual link properties (e.g., actual depth and widths of existing channels) with some equivalent links to represent several very small bayous. To aid in the

sediment distribution at a diversion, a predesigned grid of links and cells that mimics the present subdeltas in the Lower Mississippi Delta, was incorporated in the ICM. A sample link-cell layout for the Baptiste Collette subdelta is given in Figures 9 and 10. The link dimensions were estimated using a system of regime equations (e.g., Lacey, 1930, or the Colorado State University equations in Simons & Albertson, 1960). For example, the Lacey Regime Equations are:

$$P = K_1 Q^{1/2} \quad (41a)$$

$$R = K_2 \, Q^{1/3} / {f_s}^{1/3} \quad (41b)$$

$$S = K_3 \, {f_s}^{5/3} / Q^{1/6} \quad (41c)$$

$$f_s = K_{fs} \sqrt{D_{50}} \quad (41d)$$

where: P = wetted perimeter (width m);
Q = dominant discharge (m^3/s);
R = hydraulic radius (depth m);
S = energy slope;
f_s = sediment factor (see Table 2).

Typical coefficients K are given in Table 2 for channels with a sandy bed. Although the initial channel in a developing delta may be a mixture of sand, silt, and clay, it is expected that the bed will eventually become armored with sand; these coefficients were calibrated to observed dimensions of the distributary channels in the subdeltas of the Mississippi Delta (see Attachment C3-23: ICM Calibration and Validation). The regime coefficients given by Simons and Albertson (1963) demonstrate the variability of the coefficients with bed material.

Table 2: Regime coefficients for channels with sandy beds (after Lacey, 1930).

Coefficient	US (cfs)	SI (m^3/s)
K_1	2.67	4.84
K_2	0.468	0.468
K_3	0.000572	0.000316
K_{fs}	8 for D_{50} inches	1.587 for D_{50} mm

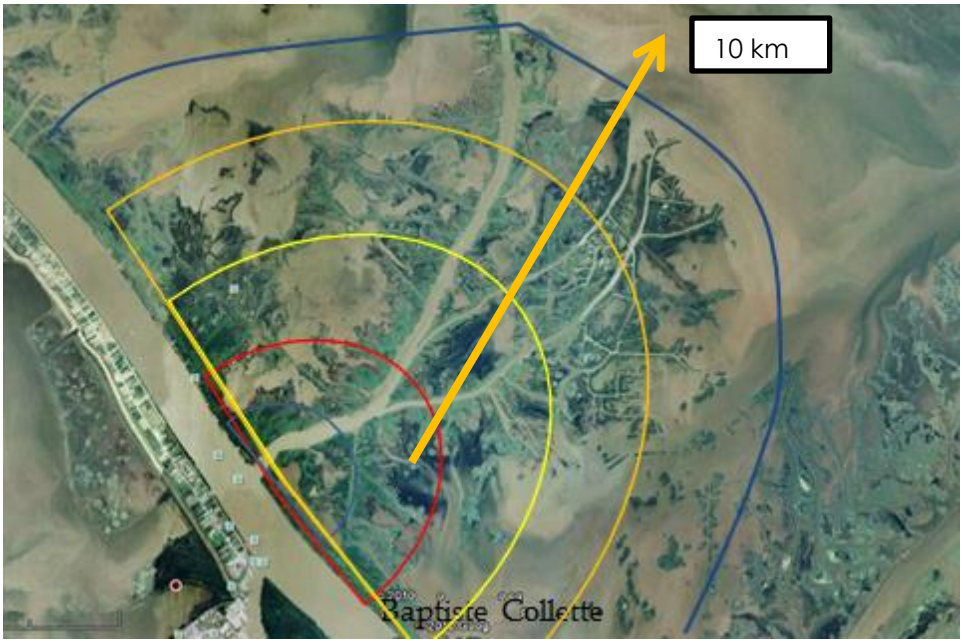

Figure 9: Example of a subdelta in the Lower Mississippi River showing bifurcations (Google Earth Image of Baptiste Collette).

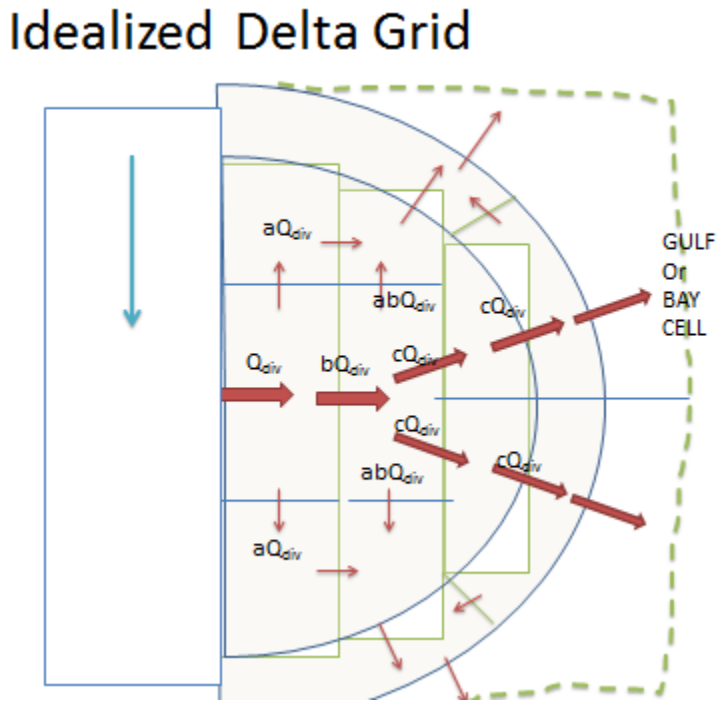

Figure 10: Stencil for delta building grid.

For silt and clay, the sediment deposition and resuspension is calculated in the open water compartments as described by Equations 4 to 11; however, Equation 1 is used to route the silt and clay sediment once it is suspended in the water column. The mass balance in Equation 1 forms the basis for the computation of the mean sediment concentration in each sediment class. Equation 1 indicates that there is an exchange within compartments between

neighboring open water cells and adjacent marsh cells. The net mass exchange rate is computed as the product of the sediment concentration at the cell face and the exchange flow, plus the diffusive exchange, which depends on the concentration gradient across the face between neighboring cells and the diffusivities in the links. The diffusivities were obtained from the salinity calibration process used for the 2012 Coastal Master Plan (CPRA, 2012; Meselhe et al., 2013).

If the open water in a given model compartment is determined to flood the compartment's marsh portion, a deposition calculation deposits sediment into the marsh interior based upon settling velocities, marsh flood depths, and flood durations. The suspended sediment concentrations in the open water portion of the compartment are reduced by this calculated marsh deposition. Refer to the Open Water-Marsh interaction section of this report for further discussion regarding distribution of deposition and erosion of marsh sediments.

2.3.1 Link Adjustments

The sediment routing process should take into account the sediment carrying capacity of the flow links that connect hydrology compartments. The suspended sediment transport capacity (in kg/s/m) for sand is calculated using Equations 32 through 40, with the White settling velocity (Equation 7). However, the hydrology subroutine does not model waves in links; only the open water compartments have a wave model. A simpler and more robust method of verifying the link conveyances is to compare the link dimensions with the regime dimensions (Equation 41). Links should be adjusted when their sediment (i.e., sand) carrying capacity is less than the sand load from the connected open water cells. It is assumed that the sand class is critical to this capacity computation since sand generally requires a greater shear stress for movement. The use of regime equations based on channels with sandy beds (e.g., Lacey, 1930) should ensure that the limiting link dimensions are sufficient to transport the sand fraction from one open water cell to the neighboring open water cell. The link dimensions are monitored and adjusted by the following rules:

$$\begin{aligned} &\text{IF } P_{link} > K_1 \,|\, Q_{link} \,|^{1/2} \quad \text{THEN } P_{link} \text{ and } R_{link} \text{ are not changed} \\ &\text{IF } P_{link} < K_1 \,|\, Q_{link} \,|^{1/2} \quad \text{THEN } P_{link} = K_1 \,|\, Q_{link} \,|^{1/2} \text{ AND } R_{link} = K_2 \,|\, Q_{link}/f_s \,|^{1/3} \end{aligned} \tag{42}$$

where Q_{link} is computed in the hydrology subroutine and the maximum annual value is used to update the links on an annual basis. The K values in Table 2 can be calibrated to the existing subdeltas.

2.4 Open Water Processes

The section summarizes the approach used for sediment distribution within the open water areas of the ICM compartments.

2.4.1 Mass Balance

Mass balance for sand, silt, and clay fractions is given by Equation 1. This is a standard mass balance formulation that has been used in many link-node models such as the Water Quality Analysis Simulation Program (WASP) models supported by the U.S. Environmental Protection Agency (2014). This approach was used in the 2012 Coastal Master Plan modeling effort.

2.4.2 Resuspension of Cohesive Sediments

Resuspension of silt and clay is modeled as described by Equations 6 to11. These equations have been used in a similar form in many sediment transport models (e.g., ECOMSED-HydroQual, 2002; Delft3d-Deltares, 2007). The 2012 Coastal Master Plan (Meselhe et al., 2013) used a similar formulation but with wind shear as a surrogate for bed shear.

2.4.3 Deposition of Sediments

The deposition rate is given by Equations 4 to 10. This formulation was first proposed by Krone (1962; 1966; 1986) and has since been incorporated in several models, such as ECOMSED-HydroQual (2002) and Delft3d-Deltares (2007). This formulation was simplified for the 2012 Coastal Master Plan by equating the settling velocity to the depositional velocity.

2.4.4 Net Resuspension and Deposition of Cohesive Sediments

The source term in Equation 1 for the silt-clay fractions is:

$$S_{r,k} = A_s \left[E_{res} - C_k V_{d,k} \right] \quad (43)$$

where: A_s = open water area (m^2); C_k = concentration of class k.

This is similar to the source term in the 2012 eco-hydrology model except for the improvements in the use of the Krone depositional velocity instead of the settling velocity and the use of the bed shear and critical shear to replace the wind shear and critical wind shear. The Young and Verhagen wave processes are given by Equations 21 to 27. A comparison by Filostrat (2014) of the results of these wave equations with those from the USACE Shore Protection Manual (USACE, 1984) indicated that they yielded very similar results. Georgiou (personal communication, 2013) found that the Young and Verhagen (1996) equations were in good agreement with his measured wave data in the open water north of the Biloxi Marsh.

2.4.5 Net Resuspension and Deposition of Noncohesive Sediments

The subroutine treats the sand transport, erosion, and deposition by defining an equivalent channel of width, b, within the open water and then by applying the van Rijn (2013) Equations 32-40. The flows are combined tidal and sub-tidal flows; however, during sand transport, in delta building areas, the mean distributary flows are expected to dominate. The van Rijn sand load gives the equilibrium sand transport load in the open water cell:

$$Q_{se} = b\, q_s \quad (44)$$

where: b = the effective width of the cell normal to direction of the maximum flow;
q_s = the van Rijn sand load for equilibrium transport.

The value of b is an open water attribute and subsequently modified in the ICM as the cell water-to-land ratio changes. An initial estimate of b is the square root of the open water area.

Three cases are possible:

a) If the bed shear stress due to waves and currents is less than the critical shear stress, then $Q_{se} = 0$ and all incoming sand load will be deposited;

b) If the bed shear stress due to waves and currents is greater than the critical shear stress, then $\Sigma Q_{sand,in} > Q_{se}$ and then deposition will occur at the rate of $\Sigma Q_{sand,in} - Q_{se}$;

c) If the bed shear stress due to waves and currents is less than the critical shear stress, then $\Sigma Q_{sand,in} < Q_{se}$ erosion will occur at the rate of $\Sigma Q_{sand,in} - Q_{se}$

where: $\Sigma Q_{sand,in}$ = the sum of the sand load entering an open water cell;
$\Sigma Q_{sand,out}$ = the sum of the sand load leaving the open water cell.

In all cases, $\Sigma Q_{sand,out} = Q_{se}$.

During the deposition phase, the effective width b will be adjusted annually based on the volume of deposition in the open water (i.e., $b_{n+1} = b_n$ – (volume of deposition)/(L_e d) where L_e is the effective length of the open water area and d is the mean depth). The width b is updated annually in the ICM.

2.4.6 Delta Building

A refined grid is introduced that permits the development of a delta at proposed diversions. A grid similar to that shown in Figure 10 was designed as a stencil for local refinement. To ensure that the links have appropriate capacity, the regime dimensions (e.g., Lacey, 1930; Simons & Albertson, 1960) formulae is used. The scale of the grid could be adjusted to account for the "river mouth bar" lengths for first order bifurcation. The research of Coleman (1988) on the subdelta of the lower Mississippi River shows the growth to a maximum radius followed by interior decay of the subdeltas. The mouth-bar interval gives a guide to the bifurcation distance and thus the scale of the grid (Esposito et al., 2013). The stencil for a delta is designed based on the expected maximum radius of the delta fan and the bifurcation scale. The links in the stencil are designed using the regime equations (Lacey, 1930) and the dominant flow in the diversion.

2.4.7 Link Adjustments

The links between the open water cells should have a capacity equal or greater than the sand load from the open water. The link depth and width is automatically updated by modifying these dimensions if they are less than the regime dimensions (Lacey, 1930). The regime modifications follow the rules in Equation 42. Regime dimensions are based on field data from fluvial channels carrying sediment (Leopold et al., 1964). Lacey's equations are appropriate since they were developed for stable sandy bed channels with relatively low sand concentrations (<100 ppm) which is applicable to the Lower Mississippi River with sand concentrations that are generally less than 100 mg/L. This approach ensures realistic link dimensions and energy losses. The regime approach is recommended over more mechanistic approaches, such as van Rijn (2013), to avoid excessive computations and the associated numerical stability problems.

3.0 Exchange between Open Water and Marsh (Excluding Hurricanes)

The compartmental processes are separated into hurricane and non-hurricane periods. Storm events that are not classified as hurricanes are modeled using the normal wind record while hurricane events have the normal wind record replaced by hurricane wind fields. The technical team examined characteristics of tropical storms and hurricanes in the existing storm suite to identify threshold characteristics for higher frequency events to be considered 'storms'. This determined the types of events which needed to be extracted from the 50-year 'base conditions' in order that 'storm conditions' could be inserted. Storm characteristics were determined and are documented in Attachment C3-3: Storms in the ICM Boundary Conditions.

In terms of sediment movement, for the periods without hurricanes, the 2012 Coastal Master Plan eco-hydrology model assumed that the sediment transfer from the open water to the marshes occurred due to resuspension of sediment in the open water areas with subsequent conveyance by inundation flow to the adjacent marshes. It was assumed that the deposition in the marsh occurred at the settling velocity of the sediment in the water column and that once deposited, resuspension did not occur. Only fine sediments were assumed to be transferred to the marsh by this process (Christiansen et al., 2000). Sand deposition was limited to the open water areas during non-tropical storm periods.

Figure 11 illustrates the open water-marsh exchange process. In the 2012 Coastal Master Plan eco-hydrology model, the mechanism for sediment exchange between open water and the marsh involved sediment resuspension in the open water and subsequent transport into the adjacent marsh during the flooding of the marsh. This flooding is caused by high stages that can result from high inflows, tides and/or wind setup. The exchange process in the 2012 Coastal Master Plan eco-hydrology model (Meselhe et al., 2013) was used as a starting point. The 2017 Coastal Master Plan integrates the calculations of the hydrologic processes, sediment distribution, and morphology through dynamic coupling of subroutines executed simultaneously with annual updates to the landscape. The sediment distribution in the hydrology subroutine will divide the marsh in two zones: near edge and interior, and will use improved marsh inflow/outflow equations. Sediment may be transferred from open water areas to the adjacent marshes or from one open water area to another via links (channels) or from one marsh to another via over-land links.

The vegetated marsh dissipates the turbulent kinetic energy (TKE) in the flood flow resulting in a quiescent depositional environment. Under non-hurricane conditions, this environment prevents resuspension (Christiansen et al., 2000). The Kadlec Equation (Equation 2) has a coefficient, *a,* that can be used to account for marsh vegetation or lack of vegetation. The Kadlec equation has suggested values based on marsh type; the parameter, a, is assigned in the marsh attributes. The marsh edge length and the marsh area are marsh attributes.

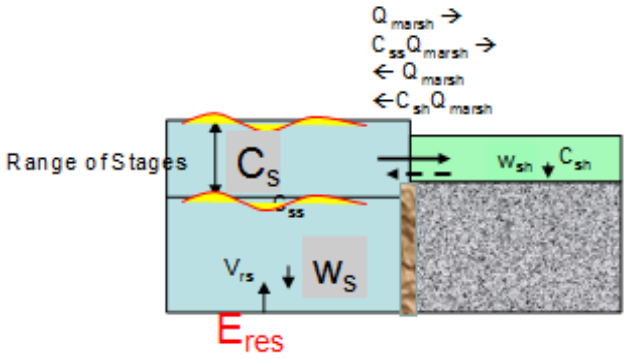

Figure 11: Open water-marsh exchange process. Q_{marsh}= flow into or out of the marsh; C_{sh} = TSS in the flooded area of the marsh; C_{ss} = TSS in the open water adjacent to the marsh; w_{sh} = settling velocity in the marsh; w_s= settling velocity in the open water; V_{rs} = resuspension velocity; E_{res} = resuspension flux.

3.1 Open Water-Marsh Exchange Modeling Approach

The relevant processes for open water-marsh exchange are described below.

Flooding phase:
The flooding phase will occur when:

Open water level > marsh elevation
AND open water level > marsh water level.

This process transports sediment into the marsh at a load:

$$Q_{s,k} = Q_{marsh}\ C_{s,k} \quad (45)$$

where: $C_{s,k}$ = open water TSS concentration by class (k) in the open water;
Q_{marsh} = flow into marsh (Equation 2).

The open water level used in Equation 2 to calculate Q_{marsh} is driven by tide, wind set up, Gulf seasonal effects, waves, and flooding due to flow-through (i.e., riverine processes). The level in the marsh is computed by Equation 1.

Ebbing Phase:
The ebbing phase will occur when:

Open water level < marsh water level
AND open water level > marsh elevation

This process removes sediment from the marsh at the rate:

$$Q_{s,k} = Q_{marsh}\ C_{s,k} \quad (46)$$

where: $C_{s,k}$ = open water TSS concentration for class (k) in the open water;
Q_{marsh} = flow out of marsh (Equation 2).

The Kadlec equation for marsh exchange flows has been used successfully in other marsh exchange applications (e.g., Arceneaux et al., 2007; Meselhe et al., 2010; Roth, 2009). This exchange equation can be calibrated for various vegetation densities/marsh types in the marshes; however, the present ICM uses a single global "a" in the Kadlec equation that is adjusted in the sediment accretion calibration procedure (see Attachment C3-23: ICM Calibration, Validation and Performance Assessment).

4.0 Sediment Processes in the Marsh Areas (Excluding Hurricanes)

The 2012 Coastal Master Plan eco-hydrology model assumed that all deposition of mineral sediment could not be resuspended. The complication of floating marshes was not included in the 2012 model.

In considering an improved method of sediment distribution across the marsh surface, it is first wise to revisit the method in which sediment was distributed within an eco-hydrology compartment of the 2012 Coastal Master Plan model. A summary of the 2012 wetland morphology model is given in Couvillion et al., 2013. In the 2012 wetland morphology model, the mineral accumulation rates from the eco-hydrology model in $g/m^2/yr$ were distributed spatially across the marsh by a raster subroutine. In that procedure, sediment accumulation rates were provided at the 2012 eco-hydrology compartment scale. Some of these compartments were relatively large scale (average coastal compartment size = 97 km^2); however, the forecast of wetland change requires calculations of accumulation at finer scales. To forecast accumulation within the hydrologic compartments at a finer scale, a sediment distribution methodology was utilized. This sediment distribution methodology is being improved for the 2017 ICM. One improvement was to sub-divide the marsh into a near edge zone and an interior zone.

The literature review (Attachment C3-1.1) identified several important marsh sedimentation processes that can be used in the improvement of the sediment distribution in the 2017 ICM. These include:

a) **Flocculation and resuspension**. Christiansen et al. (2000) found that up to 80% of the sediments entering the marsh were flocculated. For non-tropical storm conditions, they also indicated that deposited sediments were not resuspended. The sediments were predominately silts and clays. These findings are in agreement with Wang et al. (1993). Graham and Manning (2007) studied flocculation and settling velocities within a *Spartina anglica* canopy using an annular flume and floc imaging technology. The mean settling velocities exhibited inverse exponential relations with vegetation density. TSS concentrations were found to be one to two orders of magnitude lower than experienced in open water environments.

b) **Near edge turbulence effects**. Leonard and Luther (1995) showed that TKE decayed exponentially with distance from the marsh face and with the stem density as shown in Figure 12. Moskalski and Sommerfield (2012) demonstrated that the decrease in suspended solids followed a pattern similar to the TKE. This research indicates that the flood flow loses most of its TKE within 3 m of the marsh edge and reaches quiescent conditions within approximately 10 m from the marsh edge. They reported an order of

magnitude decrease in depositional rates between the marsh edge zone and the interior marsh (i.e., from 100 g/m^2/tide cycle to 10 g/m^2/tide cycle).

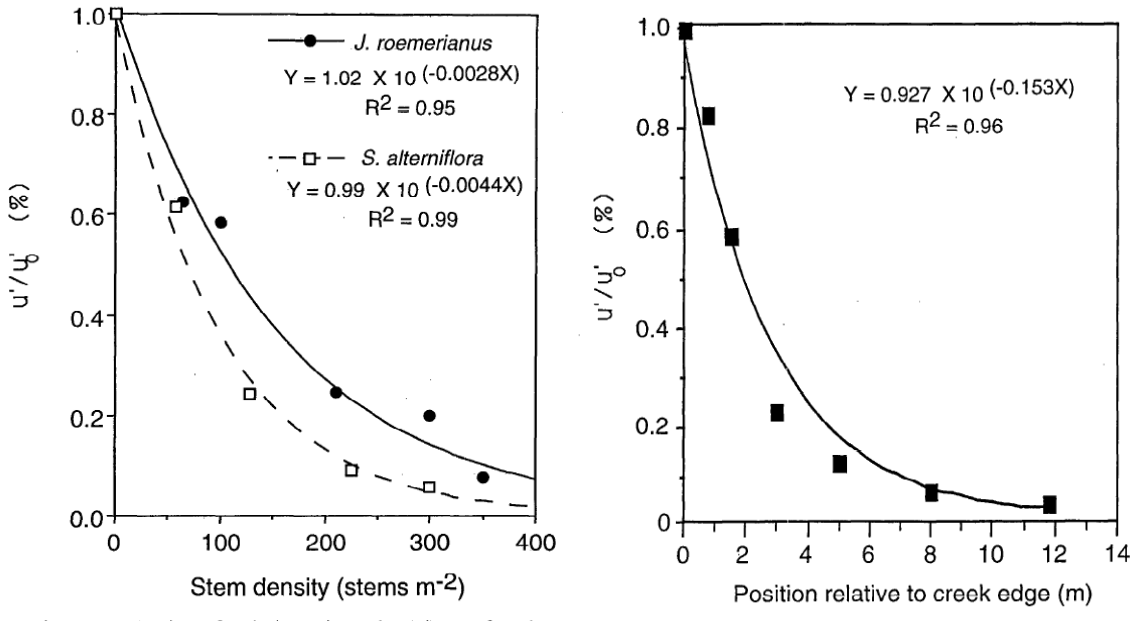

Figure 12: Decay of turbulent kinetic energy as a function of stem density (left) and setback (right) from the marsh edge (after Leonard & Luther, 1995).

c) **Near edge zone sediment distribution**. Park et al. (2012) investigated spatial deposition rates due to tidal inundation; it was found that deposition was higher at the creek bank than at the inner marsh, and decreased with distance from the estuary head. The TSS concentrations in water exported from the marsh on the ebb tide were greatly reduced compared to those delivered in the flood. Deposition rates were strongly correlated with suspended loads. Neumeier and Ciavola (2004) investigated flow resistance and sedimentation in salt marshes. They showed that the velocities through vegetation are reduced by an order of magnitude for the lower 2/3 of the height of the vegetation (Figure 13). This research also demonstrates sediment accumulations of about 5 g/m^2/tidal cycle. Coulombier et al. (2012) reported similar results on the effect of marsh canopy on the velocity distribution. Leonard et al. (1995) studied surficial sediment transport and deposition processes in a *Juncus roemerianus* marsh in west-central Florida where they monitored flow velocity, water level, TSS concentrations, and sediment deposition. It was reported that the flow velocities were inversely related to distance from the creek edge and also to stem density. The TSS concentrations near the bank were reflective of those in the tidal creek source; however, with increasing distance from the creek, current velocities decreased and a corresponding decrease in TSS concentration was observed. Rates of total deposition per tidal cycle, estimated with sediment traps, decreased from 24 g/m^2/cycle at the bank to 9.5 g/m^2/cycle 10 m into the marsh. Although winter storms tended to increase deposition rates, the overall rates for both locations (bank and 10 m into the marsh) were higher during summer than winter.

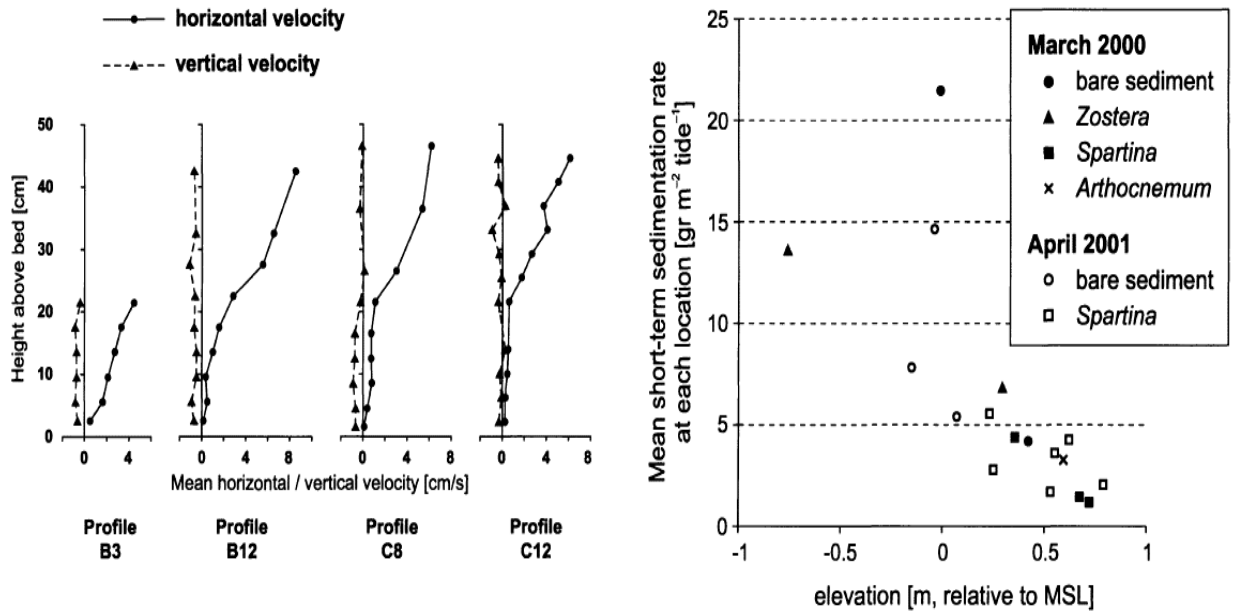

Figure 13: Velocity profiles and sedimentation in salt marshes (from Neumeier & Ciavola, 2004).

Findings such as Leonard and Luther (1995) support a two-zone approach to simulating marsh sedimentation, namely: 1) a near edge zone of approximately 10 m, and 2) an interior zone. In the near edge zone, the smaller diameter particles (i.e., clay particles and clay flocs with fall diameters < 20 um) are kept in suspension by the TKE, while the remaining fraction of the sediment tends to deposit; for practical purposes, a value of 16 um could be used for consistency with standard grain sizes. In the interior zone, the finer fraction will deposit at the settling rate of the 16 um particles. Equation 1 is applied to each sediment class to determine the mass of sediment that is removed in zones 1 and 2 respectively; the depositional velocity is set to zero in zone 1 and estimated by Equation 6 in zone 2. The hydrology subroutine computes separate annual mass accumulation rates for zones 1 and 2 that are transferred to the morphology subroutine for revising the DEM. It is necessary to use 30 m for the near edge zone to be consistent with the morphology subroutine which uses a resolution of 30 m. Figure 14 is a conceptual profile of the open water and the two marsh zones. The computational flowchart for the marsh process is presented later in this document in the section entitled "Sediment Distribution Subroutine Organization."

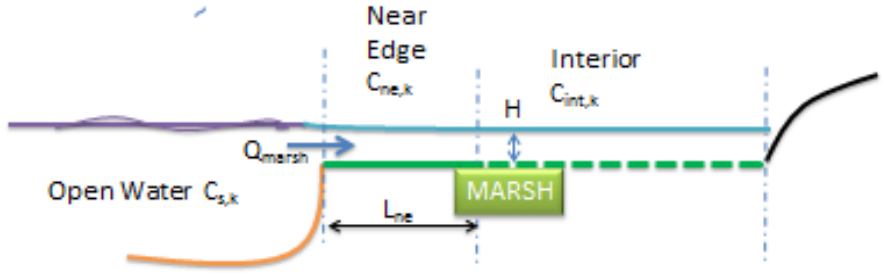

Figure 14: Definition of two-zone marsh.

4.1 Modeling Approach for Marsh Sediment Delivery

The conceptual model for the open water-marsh exchange is summarized in Figures 11 and 14. The marsh model proposed here consists of treating the marsh as two zones (i.e., near edge and interior) with the marsh-open water flow exchange given by the Kadlec Equation 2 (Kadlec et al., 1996). The literature review supports the modeling assumption that under non-hurricane stresses, the sediment deposited in the vegetated marsh is not resuspended (Christiansen et al., 2000; Wang et al., 1993). Equation 1 is applied for each zone of the marsh subcompartment with the source term computed by, which reflects the trapping efficiency of the marsh since the critical erosion shear stress is generally much higher than the bed shear stress for normal flooding and ebbing flows.

$$S_{\mathrm{r,k}} = - \, w_{\mathrm{s,k}} C_{\mathrm{sh,k}} \qquad (47)$$

The marsh depositional velocity for the clay particulate fraction in the near edge zone is reduced to zero to account for the additional turbulence and turbulent shear in the flow through the vegetated near edge zone of the marsh (Neumeier & Ciavola, 2004; Christiansen et al., 2000; Leonard & Luther, 1995; Park et al., 2012). The marsh subcompartment subroutine computes the mean accumulation rate over the near edge zone and interior marsh area. The research of Leonard and Luther (1995) shows that TKE plays a strong role in maintaining the finer and lighter solid particles in suspension; however, the TKE dissipates rapidly with distance from the marsh edge. The results of Neumeier and Ciavola (2004) confirm this finding. For consistency with land change resolution, a marsh edge zone of 10 to 30 m should be reserved for the sediments with fall velocities associated with particles larger than the clay class, approximately 16 um. This includes clay particulates and small clay flocs. The residual of the deposition is computed by applying Equation 1 to the interior marsh zone, with the assumption that the deposition is uniformly spread over the flooded portion of the interior marsh. The morphology subroutine computes the changes in the DEM of near-marsh edge zone and the interior marsh.

5.0 Sediment Processes in the Marsh Areas (During Hurricanes)

5.1 Context

In the landscape models used to support the 2012 Coastal Master Plan, the effects of tropical storms and hurricanes were considered in only a few aspects of landscape dynamics. The 2017 ICM uses the sediment distribution capabilities of the new hydrology subroutine code and extends the wind series to include hurricane events. A detailed approach for implementing storms into the landscape has been developed, which includes the identification of threshold characteristics for events to be considered storms (Attachment C3-3: Storms in the ICM Boundary Conditions). Storm conditions, including water levels, wind, precipitation, and other required parameters are used as boundary condition inputs to the ICM during storm periods. The model improvements made to support the 2017 Coastal Master Plan also enable a more explicit consideration of some storm effects such as barrier island erosion and overwash.

The 2012 Coastal Master Plan eco-hydrology model included inundation due to storm surges, but the mass transfer due to storm events appeared to be very low, possibly because this process was not well captured in the model. Consequently, a default marsh accumulation due to hurricanes was added in the 2012 wetland morphology model. Hurricane sediment accumulation was based on a constant annual sediment accumulation rate of 1,000 g/m^2. The studies of Hurricane Andrew by Cahoon et al. (1995) show deposition rates of sand, silt, and clay of the order of several centimeters; their results also suggest that the ratio of fines to sand decreases sharply with the distance inland from the coastal barrier islands. The computed hurricane sediment accumulation used in 2012 is a net value, which was assumed to account for deposition, less the erosion during the hurricane event. This section describes issues considered in the development of the ICM with respect to storm sediment distribution. Attachment C3-1.1 includes more detail on approaches which were considered but not implemented due to lack of data or other concerns.

5.1.1 Sources

The sources of sediment available for transport by storm surges are offshore continental shelf, beach and barrier islands, bay bottom, shallow water bodies (e.g., lakes and ponds), and soils in the interior marsh. The constitution of the sediments depends on where these sources originate. Consequently, sand dominated accumulation is associated with the marshes near the continental shelf or barrier islands while silt-clay dominated accumulation occurs around bays, lakes, and ponds (McKee & Cherry, 2009; Nyman et al., 1995; Tweel & Turner, 2012).

5.1.2 Processes

Processes contributing to accumulation on the marshes during hurricanes are essentially the same as those associated with non-hurricane flooding. There is, of course, a difference in the magnitude of the impact and in the composition of the accumulated sediment. The other issue (uncertainty) that should be noted is the potential for wave induced shear stresses during a hurricane to be substantial enough to cause erosion of the marsh surface and marsh edge.

5.1.3 Magnitude and Distribution

The magnitude and spatial distribution of hurricane-induced accumulation on wetland surfaces are spatially heterogeneous and discontinuous. Field investigations found that across Louisiana wetlands the maximum sediment thickness was 85 cm (Williams, 2012), and the maximum mass deposition rate was 28.6 g/cm^2 (Katrina, Turner et al., 2006). Hurricanes can bring sediments to wetlands as far as 214 km from the storm track (Ike, Tweel & Turner, 2012), and as far as 43 km from coastlines (Katrina, Tweel & Turner, 2012).

5.1.4 Controlling Factors

Controlling factors for storm sediment magnitude and distribution can be grouped into three categories: 1) storm features (e.g., storm track, landfall location, forward speed, hurricane-induced wind speed, wind direction, wave and storm surge), 2) landscape features (location relative to storm track, distance to storm track, distance to coastline), and 3) vegetation and local morphological features (plant biomass, stem density, community types, etc.; Williams & Flanagan, 2009; Tweel & Turner, 2012; Williams, 2012).

5.1.4.1 Return Period

Patterns of storm impacts in space and time to be used for the 50-year ICM simulation were identified as part of the development of the storms in the landscape approach (Attachment C3-3: Storms in the ICM Boundary Conditions). Integration of tropical storm events into the ICM would ideally be consistent across the relevant subroutines: barrier islands, hydrology and morphology.

5.1.5 Calculating Sediment Contribution

The 2012 Coastal Master Plan models included a generalized appreciation of marsh sediment accumulation associated with storms. Storm induced sediment deposition was represented by a constant annual sediment accumulation rate of 1,000 g/m^2. Spatially homogeneous sediment deposition is a known inaccuracy and as such, a means of reflecting that variability, both spatially and among storms, was sought for the 2017 ICM. Field investigations of Louisiana wetlands that examined the effects of individual storms found that the maximum sediment thickness was 85 cm (Ike, Williams, 2012), and the maximum mass deposition rate per storm was 286,000 g/m^2 (Katrina, Turner et al., 2006).

Any approach used in the 2017 ICM that reflects gradients of sediment deposition with individual storms is likely to be challenged by the lack of data for storms of different magnitudes. In recent years, there have been detailed studies of a few storms in terms of their effect on sediment distribution (e.g., Turner et al., 2006). However, these storms do not reflect the range of storm 'magnitudes' being considered for the ICM.

5.2 Approach Adopted

Attachment C3-1.1 describes research by Tweel and Turner (2012, 2014) on the spatial distribution of sediment distribution associated with hurricanes. Applying those relationships in the ICM would require major assumptions about the relationship between the few historical storms for which sediment loads have been measured and those simulated in the 50-year model runs. The final sediment distribution mechanism applied in the ICM for storm conditions uses the same general approach as for non-storm conditions (e.g., forcing from waves and currents resuspends sediment which is then distributed from open water areas of the compartment to marsh areas according to the relationships described in this report). However, two important limitations were also imposed to prevent excessive levels of TSS during periods of storm forcing:

- TSS is limited to a maximum value of 250 mg/l (all sediment size classes combined) by turning off bed resuspension when the limit is reached.
- A limit is set on the mass of sediment which can be resuspended during each year. For inshore open water areas, this is set at the mass of mineral sediment that is equivalent to a depth of 5 cm of sediment (not accounting for sediment bulk density).

Further testing and refinement of these approaches occurred during calibration and validation of the hydrology subroutine (Attachment C3-23: ICM Calibration, Validation and Performance Assessment).

6.0 Contribution of Marsh Edge Erosion to the Sediment Mass Balance

One source of sediment for the open water is the material from marsh edge erosion. The output of the marsh edge erosion calculations (Attachment C3-2: Marsh Edge Erosion) forms part of the sediment mass balance for both the open water and the marsh subcomponents.

Based on historical marsh edge erosion rates, an annual volume of edge erosion is calculated. The marsh composition is used to assign the mass contribution of sand, silt, and clay to the mass balance. The conversion of volume to mass is computed based on the mineral content of the marsh; this depends on the void ratio or bulk density, the organic content, and the mineral content of the eroding marsh. This information is derived using the approach described in Attachment C3-2: Marsh Edge Erosion.

The split of the mass between open water and marsh is treated as a function of $(d + H_s/2)/h$ where d is water depth at the marsh edge, h is the marsh height and H_s is the significant wave height (Figure 15).

For example,

- $(d + H_s/2) / h < 1$; 100% of sediment to open water (sand, silt, clay, floc)
- $d/h > 1$; 100% of sediment to marsh during positive flow to the marsh (sand, silt, clay, floc)
- $(d + H_s/2) / h > 1$ and $d/h < 1$, transition from 100% open water to 100% marsh.

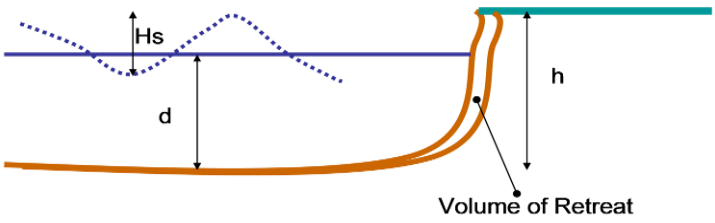

Figure 15: Some factors affecting the distribution of marsh edge erosional material.

7.0 Sediment Distribution Code Organization

Sediment distribution processes are coded within the broader hydrology subroutine in the ICM. The hydrology subroutine computes the water flow, stage, salinity, water temperature, sediment concentrations, nutrients, and algae within the ICM. A flowchart for the hydrology subroutine is shown in Figure 16.

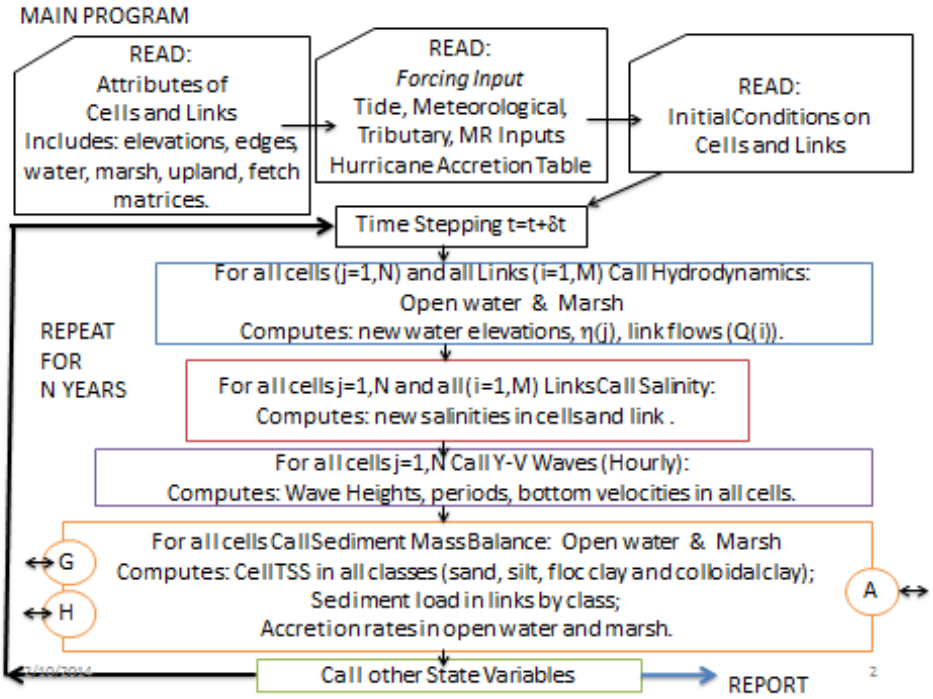

Figure 16: Flowchart for the hydrology subroutine of the ICM.

The open water sediment processes are outlined in the flowchart in Figure 17. These processes are called from the hydrology subroutine at (G). The procedure is to apply the mass balance equation to each class of sediment.

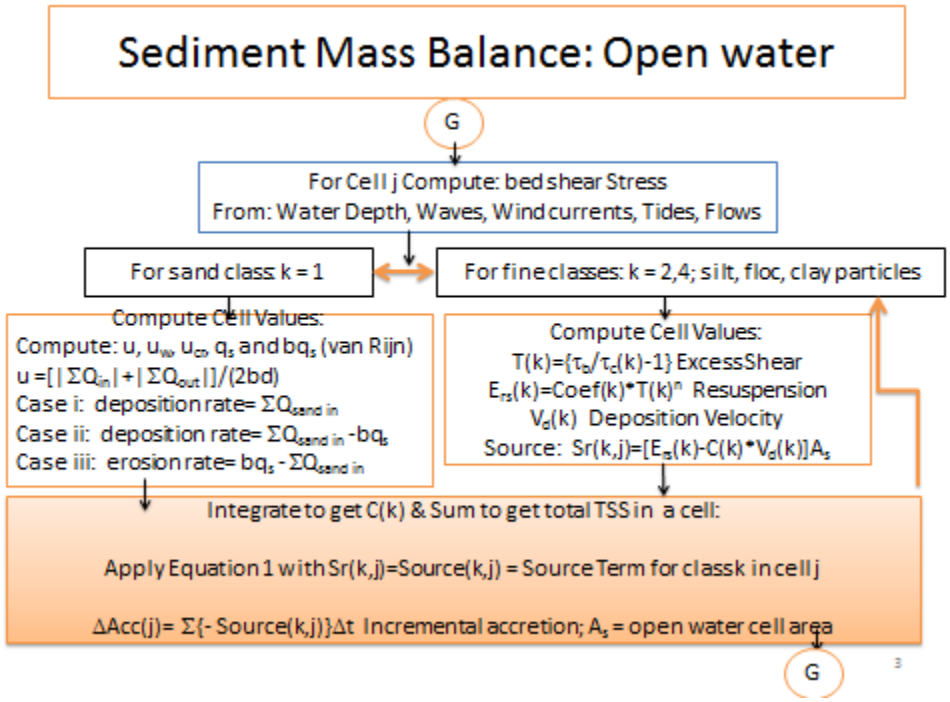

Figure 17: Flowchart for open water sediment processes.

A flowchart for the marsh, similar to that for open water, is called at (H) in Figure 16. Figure 18 shows the marsh sediment coding. The inorganic sediment from the marsh edge erosion subroutine is introduced as a source to Equation 1 on an annual basis (Figure 19). Figure 20 shows the integration of the wind data (speed and direction) with the fetch array for each open water cell to obtain the wave period and height to be used in the cohesive sediment resuspension and deposition processes and the sand transport, erosion, or deposition. A 16-direction fetch array was provided for the open water cell. The wind speed and direction record was mapped into the 16-direction classes in the fetch array as illustrated in Figure 20. First the wind time series (speed and direction) is read and used with 16-bin look-up tables for fetch. The wind direction is converted to a bin index corresponding to one of 16 fetch bins in the look-up file. Then the speed, fetch and depth are used in the Young and Verhagen equations. A 16-direction fetch array was provided for the open water cell. The wind speed and direction record was mapped into the 16-direction classes in the fetch array as illustrated in Figure 20. Pre-set arrays for mean depth and fetch are used as look-up tables while the wind speed and wind direction are input as time series.

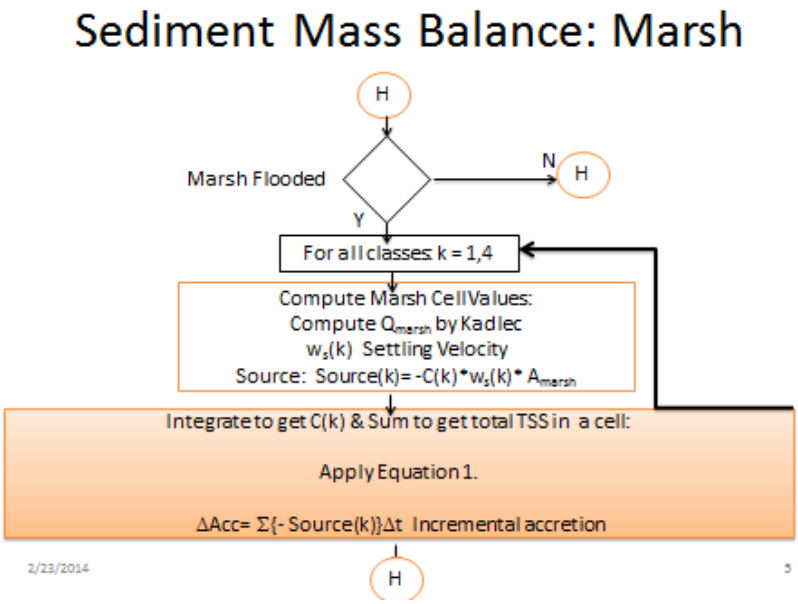

Figure 18: Flowchart for marsh processes.

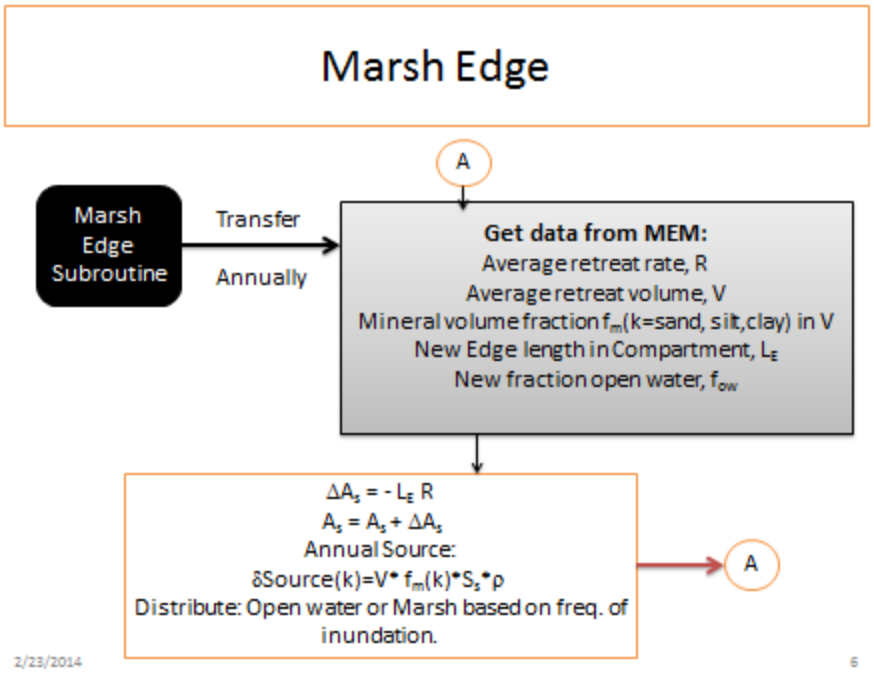

Figure 19: Annual corrections of open water area and accumulation for marsh edge retreat.

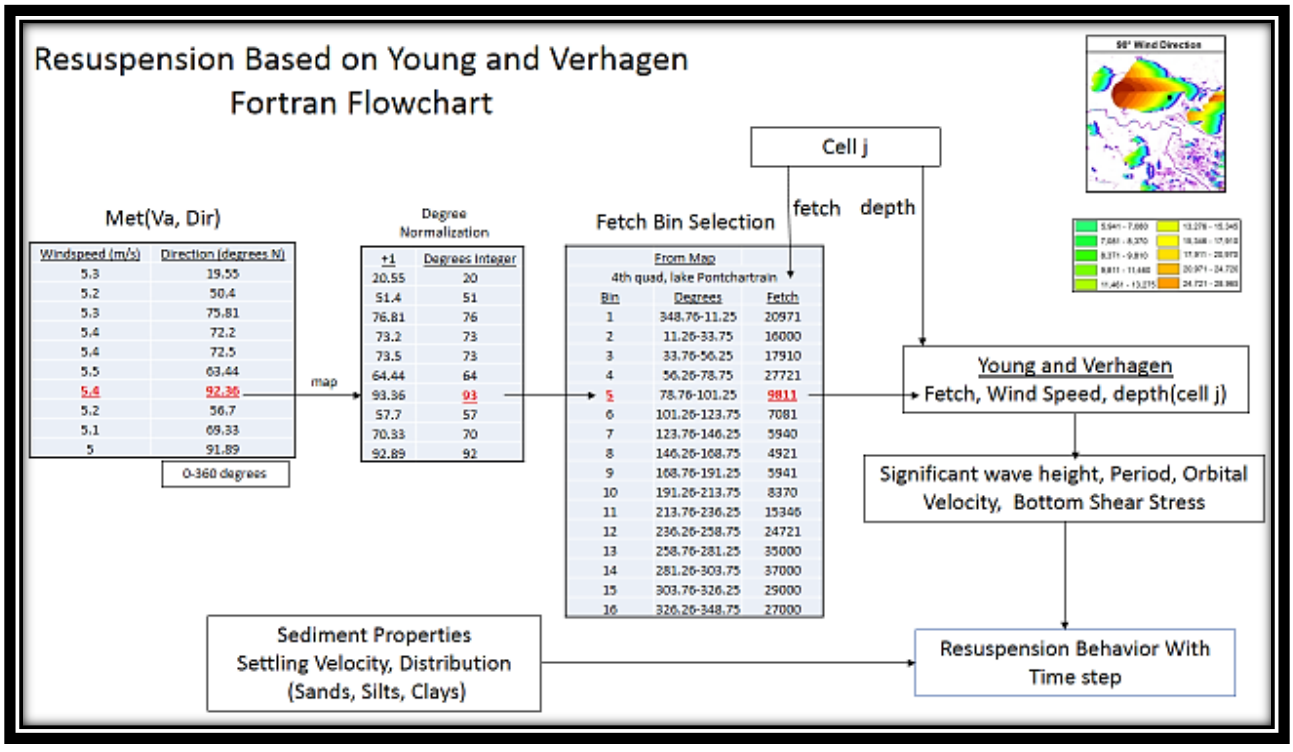

Figure 20: Integration of wave model with open water sedimentation.

The flowchart for the two-zone marsh accumulation is shown in Figure 21. The input to the marsh is determined by the product of the open water concentrations and the flow into the marsh as

computed by Equation 2. The atmospheric contribution per unit area to the water balance in all subcompartments (open water, marsh and upland) is estimated by {Rainfall rate – evapotranspiration rate}. Equation 1 is applied to both the near edge and interior zones. The fine sediment (clay particulate) is assigned a deposition velocity of zero in the near edge zone. Both zones are assumed to have no resuspension for non-hurricane conditions. The sediment that does not deposit in either the near edge or interior zone is returned to the open water.

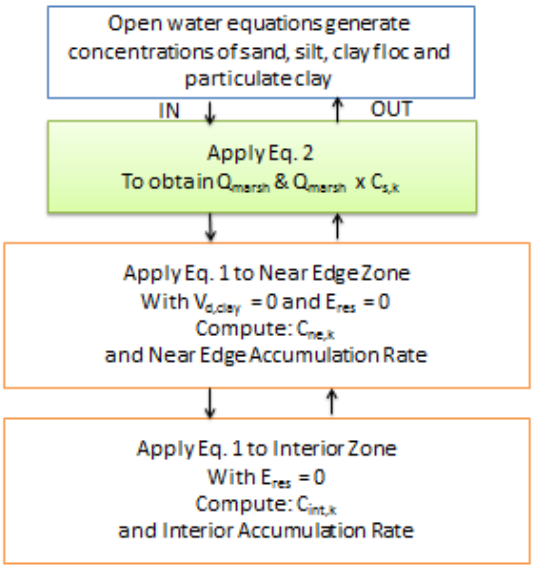

Figure 21: Two-zone treatment of marsh accumulation.

8.0 Code Testing

Figure 22 was developed by Filostrat (2014) to test the integration of the sediment distribution equations outlined in Section 7 (and shown in Figure 20) for a cell in the southeast quadrant of Lake Pontchartrain. Noncohesive and cohesive fractions were included and results found that the TSS response for cohesive sediments was stable at timesteps on the order of 60 seconds; Equations 32 to 40 were used for sand load and equations 10 and 11 for the cohesive sediment load. A sample of the results of these tests are provided in Figure 22 for a wind with U10 = 5.5 to 4 m/s for 24 hours followed by a calm period.

Filostrat (2014) also tested the proposed equations for a hypothetical diversion into an open water cell with an area of 15 km^2 and an initial effective width of 3 km and an average depth of 3 m. A pulsed diversion with a peak flow of 1,200 m^3/s with 10 mg/L sand, 10 mg/L silt, 60 mg/L flocculated clay and 20 mg/L particulate clay. This was run to demonstrate the capability of the van Rijn (2013) equations (32-40) to simulate the net accumulation rate of noncohesive sediment. A daily wind record from the New Orleans Airport was used in the wave computations. Figure 23 shows the hypothetical receiving water for a pulsed diversion. Figure 24 shows the initial sand accumulation rate in $kg/m^2/d$, while Figure 25 shows the accumulation rate after the cell width has been reduced to an effective width of approximately 300 m due to infilling. This test indicated that the proposed treatment of sand transport in a cell with a diversion will result in progressive bypassing of sand as the cell experiences land building.

A similar testing procedure was also conducted for the marsh-open water exchange flows Q_{marsh}, to be estimated with the Kadlec-Knight power law model (Equation 2). A spreadsheet

analysis was conducted which intermittently flooded and drained a theoretical marsh from an assumed tidal signal. The results from this test case are provided in Figure 26. For this test, the mean marsh elevation was 0.2 m and the mean open water level was 0.1 m.

These theoretical marsh exchange flow rates were also used to test the intra-marsh sediment deposition equations proposed in this document (Equations 1 and 47). Figures 27, 28, and 29 provide the results of this two-zone marsh deposition test. In this test, the near edge zone was set at 30 m to be consistent with 30 m raster imagery used to map the DEM. The results show that the near edge zone tends to accumulate at a much higher rate than the interior of the marsh.

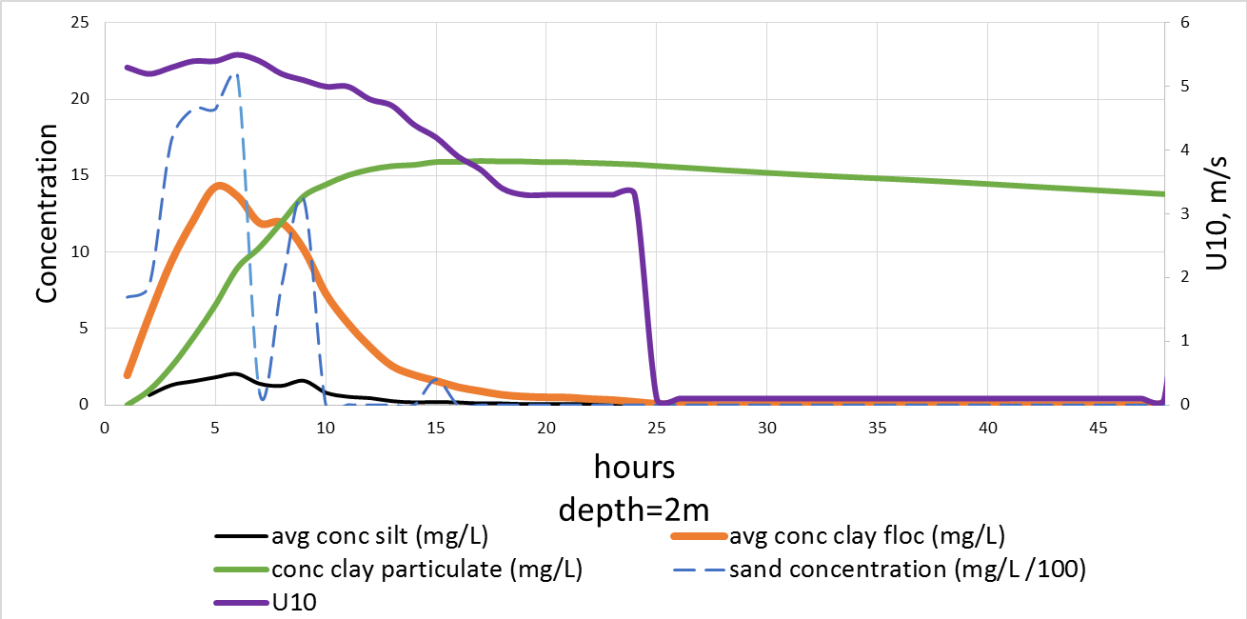

Figure 22: Suspended sediment response to a wind blowing for 24 hours in the southeast cell of Lake Pontchartrain (Filostrat, 2014).

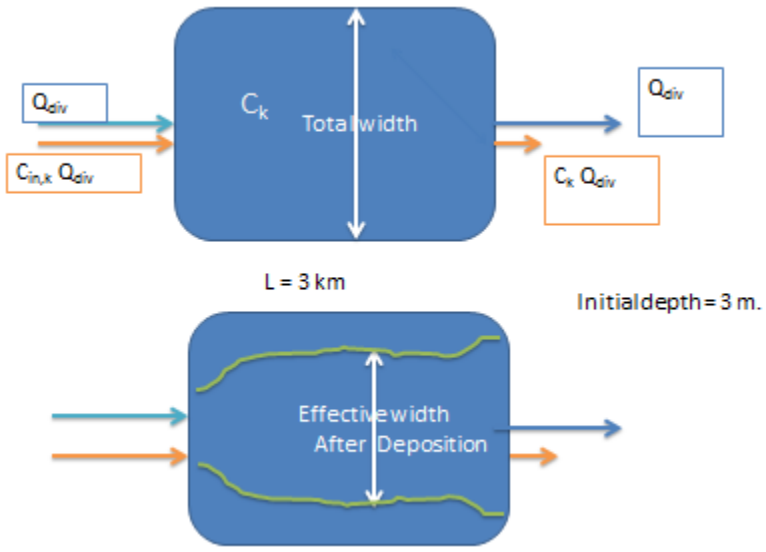

Figure 23: Test for sand accumulation at a diversion.

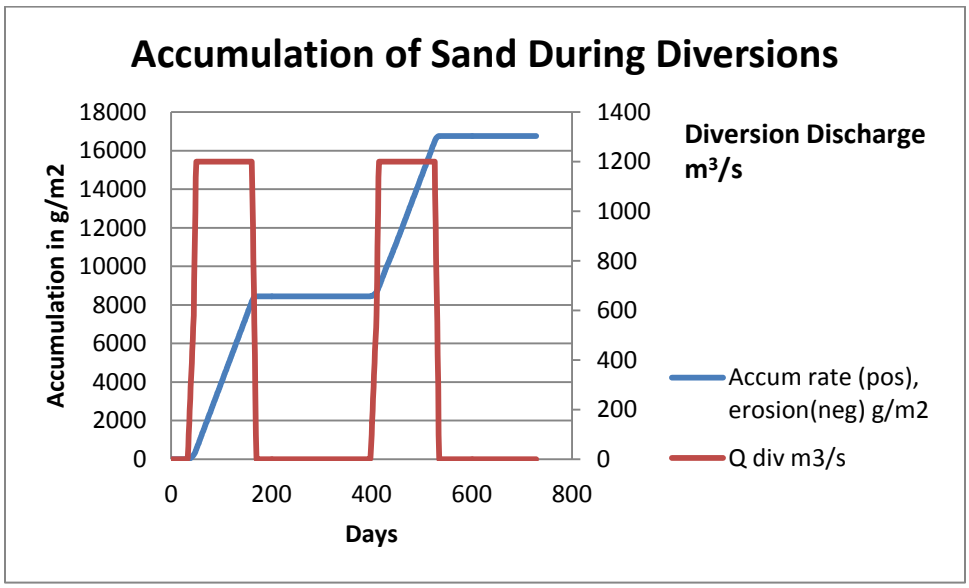

Figure 24: Sand accumulation rate for a pulsed diversion before land-building.

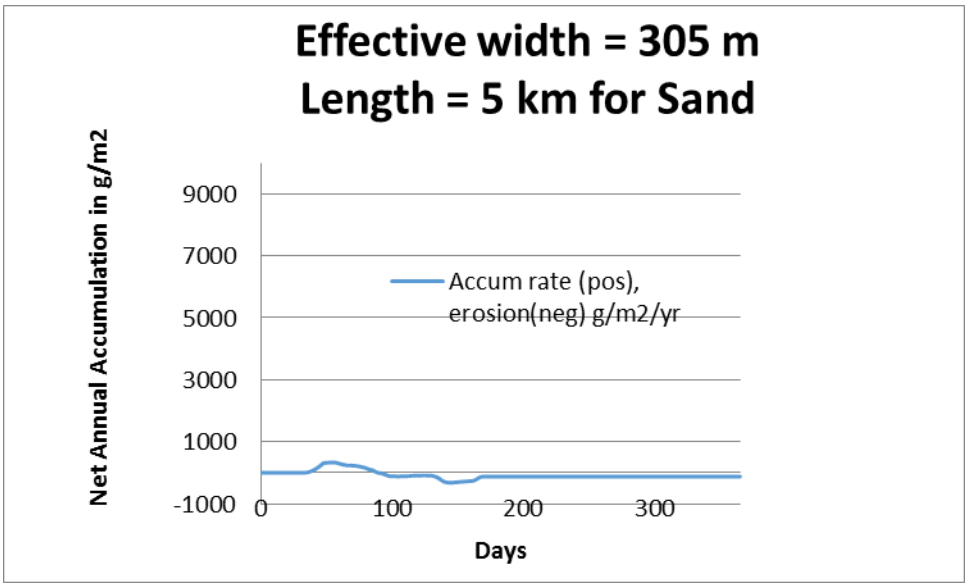

Figure 25: Sand accumulation rate for a pulsed diversion after land-building.

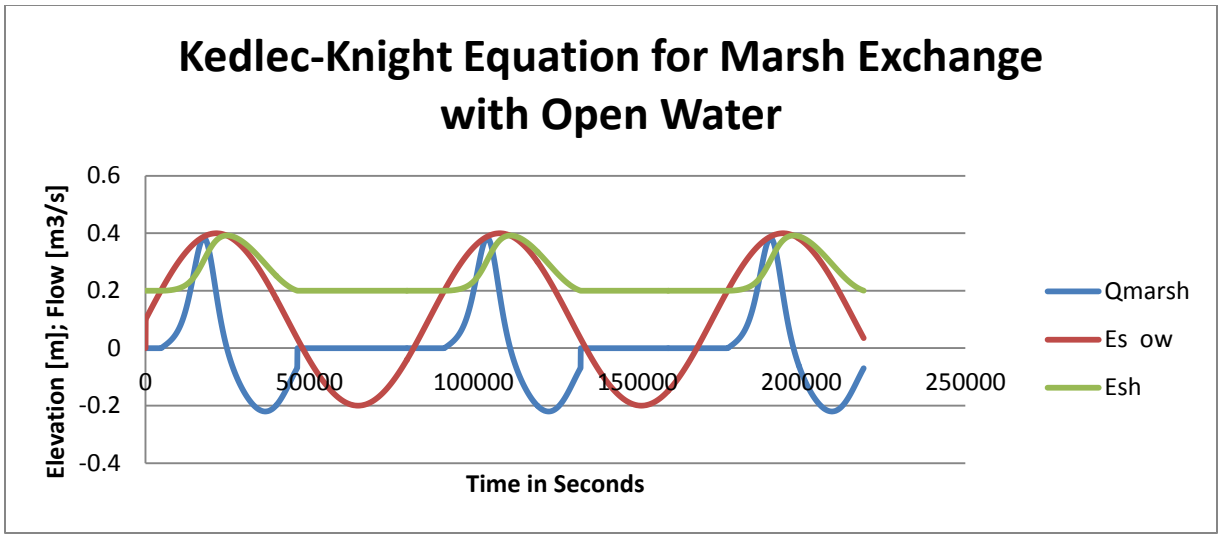

Figure 26: Marsh stage response to tidal forcing in the open water; testing the Kadlec-Knight equation. 'Qmarsh' (blue) is exchange flow (m^3/s), 'Es ow' (red) is open water level elevation, and 'Esh' (green) is marsh water elevation.

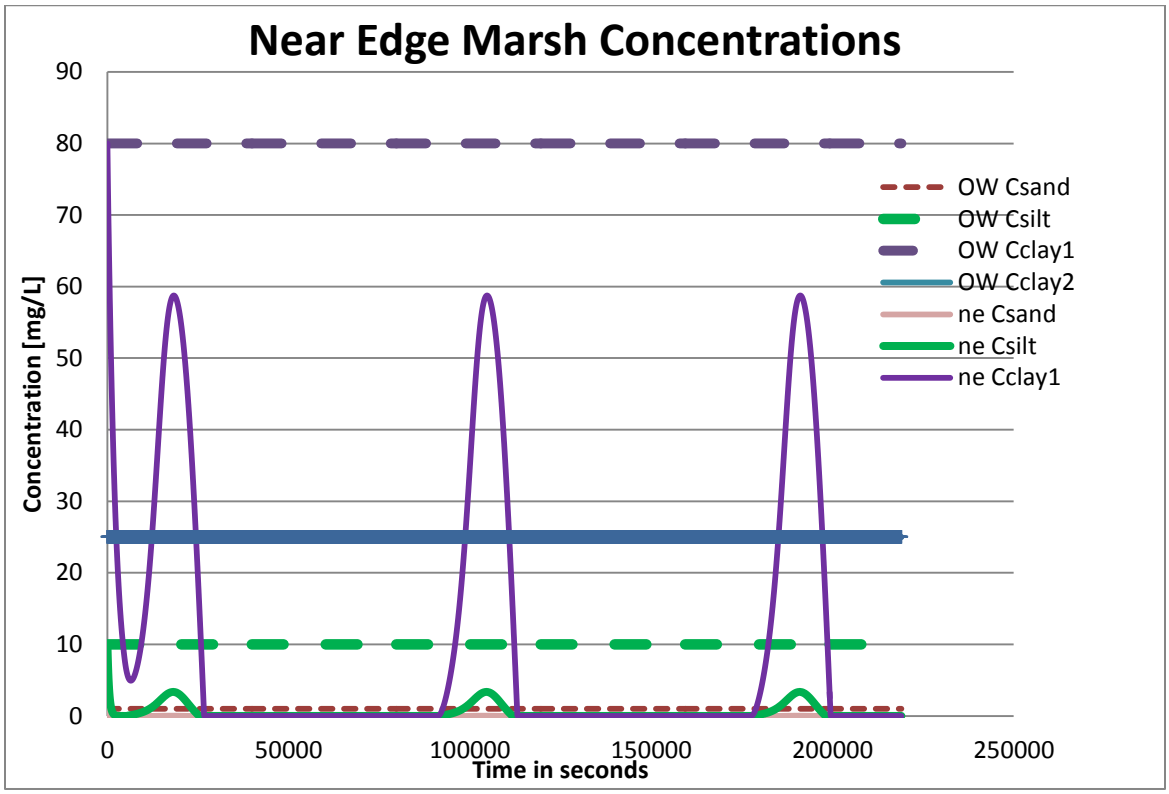

Figure 27: Suspended sediment response to tidal flooding of the near edge marsh: testing the two-zone marsh concept. 'OW' is the concentration in the open water of suspended sediment, and 'ne' is the concentration (C) in near edge marsh zone of suspended sediment. The four particle classes (sand, silt, nonflocculated clay [clay2], and flocculated clay [clay1]) are included in this figure.

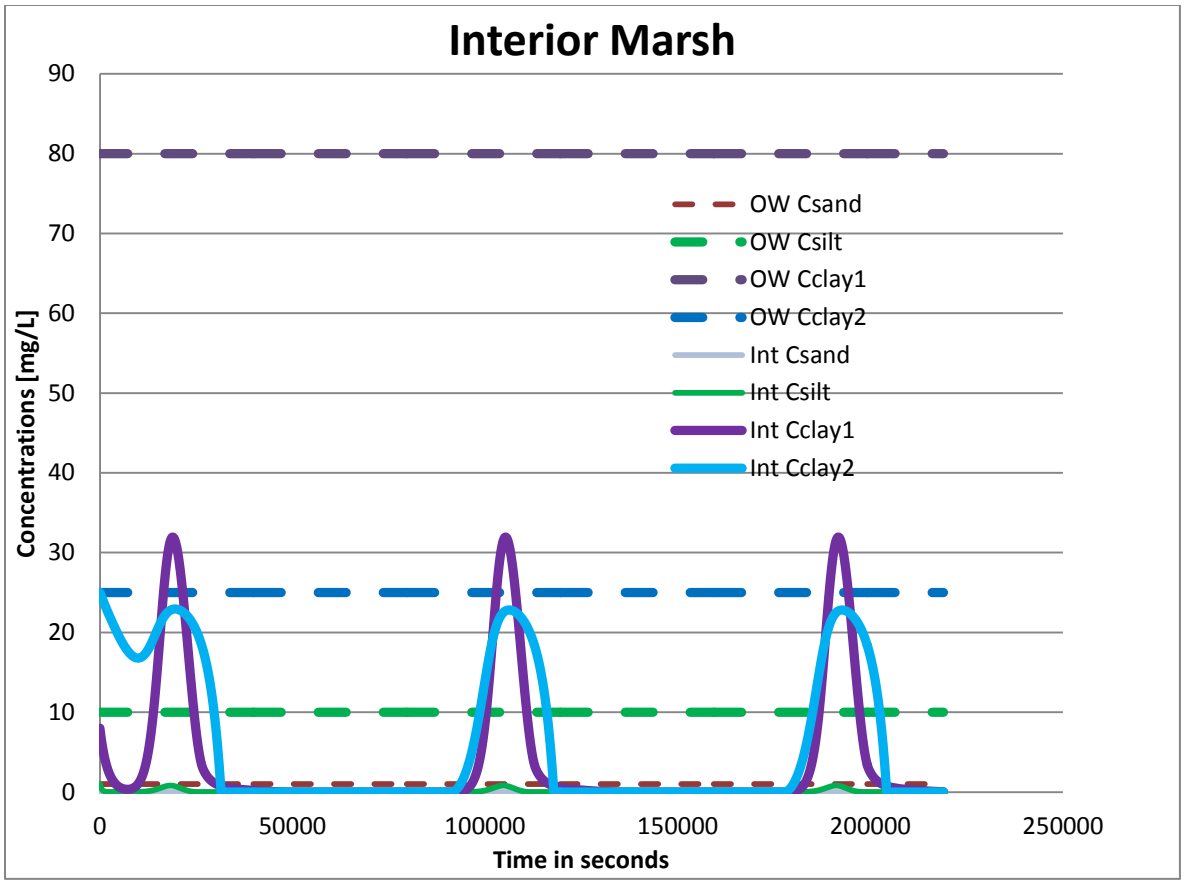

Figure 28: Suspended sediment response to tidal flooding of the interior marsh: testing the two-zone marsh concept. 'OW' is the concentration in the open water of suspended sediment, and 'Int' is the concentration (C) in the interior marsh of suspended sediment. The four particle classes (sand, silt, nonflocculated clay [clay2], and flocculated clay [clay1]) are included in this figure.

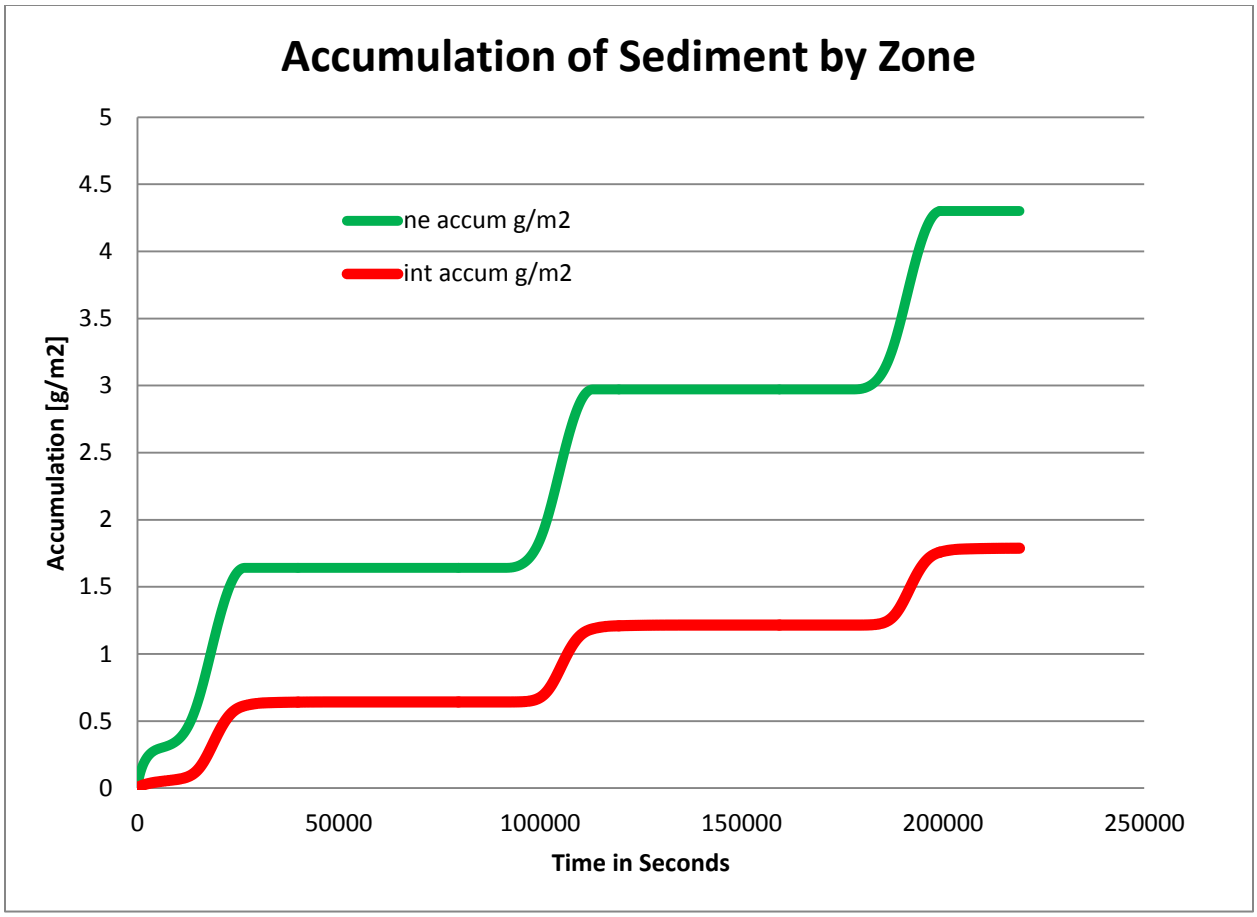

Figure 29: Suspended sediment response as cumulative accumulation to tidal flooding of the marsh: testing the two-zone marsh concept. 'ne' = near edge (green), 'int' = marsh interior (red).

9.0 References

Ackers, P. and White, W.R. (1975). Sediment transport, new approach and analysis. ASCE, *Journal of Hydraulic Div.*, *99*(11).

Anderson, F.E. (1970). The periodic cycle of particulate matter in a shallow, temperate estuary. *Sediment Petrology, 40*, 1128-1135.

Anderson, F.E. (1972). Resuspension of estuarine sediments by small amplitude waves. *Sedimentary Petrology, 42(*3), 602-607.

Arceneaux, J., Meselhe, E.A., Griborio, A., and Waldon, M.G. (2007). *The A.R.M Loxahatchee National wildlife refuge water budget and water quality models.* Report No. LOXA-07-004. Retrieved from http://mwaldon.com/LoxModel/reports/LOXA07-004--2007-06.pdf

Bacon, M.P. (1994). Pb balance and implications for particle transport on the continental shelf, U.S. Middle Atlantic Bright. *Deep Sea Research, 41*(Part II), 511-535.

Biscaye, P.E. (1988). Fluxes of particles and constituents to the eastern U.S. continental slope and rise: SEEP-I. *Cont. Shelf Research, 8*, 855-904.

Blom, G., and Aalderink, R.H. (1998). Calibration of three resuspension/sedimentation models. *Water Science Tech, 37*(3), 41-49.

Booth, J.G., Miller, R.L., McKee, B.A., and Leathers, R.A. (2000). Wind induced sediment resuspension in a microtidal estuary. *Continental Shelf Research, 20*(7), 785-806.

Cahoon, D.R., Reed, D.J., Day, J.W., Boumans, R.M., Lynch, J.C., McNally, D. and Latif, N. (1995). The influence of Hurricane Andrew on sediment distribution in Louisiana coastal marshes. *Journal of Coastal Research. 18*, 280-294.

Chang, G.C., Dickey, T.D., and Williams, A.J. (2001). Sediment resuspension over a continental shelf during Hurricanes Edouard and Hortense. *Journal of Geophysical Research, 106* (C5), 9517-9531.

Christiansen, T., Wiberg, P.L. and Milligan, T.G. (2000). Flow and sediment transport on a tidal salt marsh surface. *Estuarine, Coastal and Shelf Science, 50*, 315-331.

Cobell, Z., Zhao, H., Roberts, H.J., Clark, F.R. and Zou, S. (2013). Surge and wave modeling for the Louisiana 2012 Coastal Master Plan. In: Peyronnin, N.S. and Reed D.J. (eds.), Louisiana's 2012 Coastal Master Plan Technical Analysis. *Journal of Coastal Research, 67,* 88-108.

Coleman, J.M. (1988). Dynamic changes and processes in the Mississippi Delta. *Geological Society of America Bulletin*, *100(7)*, 999-1015.

Coulombier, T., Neumeier, U., and Bernatchez, P. (2012). Sediment transport in a cold climate salt marsh (St. Lawrence Estuary, Canada), the importance of vegetation and waves. *Estuarine, Coastal and Shelf Science, 101*, 64-75.

Couvillion, B.R., Steyer, G.D., Wang, H., Beck, H.J., and Rybczyk J.M. (2013). Forecasting the effects of coastal protection and restoration projects on wetland morphology in coastal Louisiana under multiple environmental uncertainty scenarios. In: Peyronnin, N.S. and Reed D.J. (eds.), Louisiana's 2012 Coastal Master Plan Technical Analysis. *Journal of Coastal Research, 67,* 29-50.

CPRA. (2012). *Coastal Master Plan: Appendix D-1 - Eco-hydrology model technical report*. Retrieved from http://www.coastalmasterplan.la.gov/

CPRA. (2013). *2017 Coastal Master Plan: Model Improvement Plan.* Version II (March 2014), prepared by The Water Institute of the Gulf. Baton Rouge, Louisiana: Coastal Protection and Restoration Authority, 52p.

Deltares. (2013). Sediment transport and morphology. Delft3D-FLOW: Simulation of multi-dimensional hydrodynamic flows and transport phenomena, including sediments. *User Manual, Hydro-Morphodynamics.* (Ver. 3.15.30059).

Demirbilek, Z., and Vincent, C.L. (2002). Wave water mechanics. Coastal Engineering Manual, Part II, Water Wave Mechanics, Ch. II-1, Engineer Manual 1110-2-1100, *U.S. Army Corps of Engineers, Washington, DC*.

Dupuis, Anis (2013) Observations and Modeling of Wind Waves in a Shallow Estuary: Galveston Bay, Texas, Journal of Waterway, Port, Coastal and Ocean Engineering, Vol. 139, No. 4, July/August 2013, pp. 314-325,

Ekman, V. W. (1905). On the influence of earth's rotation on ocean currents, *Ark. F. Mat. Astr. Och Fysik., Stockholm*, *2*(11), 1-52.

Erm, A., Alari, V., and Kask, J. (2011). Resuspension of sediment in a semi-sheltered bay due to wind waves and fast ferry wakes. *Boreal Environmental Research, 16, Supp. A*, 149-163.

Esposito, C., Georgiou, I.Y., and Kolker, A. (2013). Hydrodynamic and geomorphic controls on mouth bars evolution. Geophysical Res. Letters, 40, 1-6.

Filostrat, J. (2014). Estimation of Sediment Resuspension and Deposition in Coastal Waters. Master of Science Thesis submitted to the Department of Civil and Environmental Engineering, University of New Orleans.

Georgiou, I., McCorquodale, A. and Crowder, K. (2007). *Rapid prototyping of NASA MODIS 250 m data in the calibration/validation of a sediment transport model for water quality assessment and public health decision support*. Report Submitted to Richard Miller, Ph.D. National Aeronautics and Space Administration Science and Technology Division EA41. Stennis Space Center, MS 39529.

Glenn, S.M. (1987). A suspended sediment stratification correction for combined wave and current flows. *Geophys Research, 92*, 8244-8264.

Graham, G.W., and Manning, A.J. (2007). Floc and settling velocity within a *Spartina anglica* canopy. *Continental Shelf Research, 27*,1060-1079.

Grant, W.D. (1979). Combined wave and current interaction with a rough bottom. *Geophys Res., 84*, 1797-1808.

Haralampides, K. (2000). A study of the hydrodynamics and salinity regimes of the Lake Pontchartrain system. (Ph.D. dissertation). Engineering and Applied Science, Department of Civil and Environmental Engineering, University of New Orleans, New Orleans, LA.

HydroQual Inc. (2002). *A primer for ECOMSED*. User's Manual, Ver. 1.3. HydroQual Inc., Mahwah, NJ, pp. 188.

Jerolleman, D. (2014). *Resuspension of coastal sediments*. (Unpublished Master's Report). Department of Civil and Environmental Engineering, University of New Orleans, New Orleans, LA.

Kadlec, R.H. and Knight, R.L. (1996). *Treatment wetlands*. Boca Raton, FL: CRC - Lewis Publishers.

Kelderman, P., De Rozari, P., Mukhopadhyay, S., and Ang'weya, R. O. (2012). Sediment dynamics in shallow Lake Markermeer, The Netherlands: field/laboratory surveys and first results for a 3-D suspended solids model. *Water Science and Technology, 66*(9), 1984-1990.

Keulegan, G.H. (1951). Wind tides in small closed channels, J. Res. *National Bureau of Standards*, *46*, 358-381.

King, D.B., and Galvin, C.J. (2002). Coastal sediment properties. Coastal Engineering Manual, Part III, Coastal Sediment Properties, Chapter III-1, Engineer Manual 1110-2-1100. *U.S. Army Corps of Engineers, Washington, DC*.

Kotylar, L.S., Sparks, B.D., and Schutte, R. (1996). Effect of salt on the flocculation behaviour of nano particles in oil sands fines railings. *Clays and Clay Minerals, 44*(1), 121-131.

Krone, R.B. (1962). *Flume studies of the transport of sediment in estuarial shoaling processes final report. Hydr. Engrg Lab. Univ. of California,* Berkeley, CA.

Krone, R.B. (1966). Predicted suspended sediment inflows to the San Francisco bay system. *Central Pacific River Basins Comprehensive Water Pollution Project*, *133*. Federal Water Pollution Control Administration, Southwest Region.

Krone, R.B. (1986). The significance of aggregate properties to transport. In A.J. Mehta (Ed.), *Estuarine Cohesive Transport Dynamics (*pp.66-84). Berlin, Germany: Springer-Verlag.

Lacey, G. (1930). Stable channel in alluvium. *Proc. Inst. Civ. Eng., 229*, London.

Lathrop, R.G., Lillesand, T.M., and Yandell, B.S. (1991). Testing the utility of simple mutli-date Thematic Mapper calibration algorithms for monitoring turbid inland waters. *International Journal of Remote Sensing*, *12*(10), 2045-2063.

Lee, C., Schwab, D. J., and Hawley, N. (2005). Sensitivity analysis of sediment resuspension parameters in coastal area of southern Lake Michigan. *Geophysical Research, 110*.

Leonard, L.A. and Luther, M.E. (1995). Flow hydrodynamics in tidal marsh canopies. Limnology and Oceanography 30:1474-1484.

Leonard, L.A., Hine, A.C., and Luther, M.E. (1995). Surficial sediment transport and deposition processes in a *Juncus roemerianus* marsh, west-central Florida. *Journal of Coastal Research, 11*, 322-336.

Leopold, L.B., Wolman, M.G., and Miller, J.P. (1964). *Fluvial Processes in Geomorphology*. San Francisco, CA: Freeman and Co.

Lynn, V.D. (1990). Sediment movement along the U.S. east coast continental shelf, I, Estimates of bottom stress using the Grant-Madsen model and near-bottom wave and current measurements. *Cont. Shelf Research, 10*, 397-428.

Mebust, C. (2015). "Analysis of sedimentation characteristics of dredged sediment used in coastal restoration and marsh creation projects", MS Thesis, University of New Orleans. May 2015.

Marani, M., D'Alpoas, A., Lanzoni, S. and Santalucia, M. (2011). Understanding and predicting wave erosion of marsh edges. *Geophysical Research Letters*, *38*, L21401.

McAnally, W.H., Friedrichs, C., Hamilton, D., Hayter, E., Shrestha, P., Rodriguez, H., and ... Teeter, A. (2007). Management of fluid mud in estuaries, bays, and lakes. I: Present state of understanding on character and behavior. *Journal of Hydraulic Engineering*, 133(1), 9-22.

McCorquodale, J.A., Roblin, R., Georgiou, I.Y. and Haralampides, K. (2009). Salinity, nutrient and sediment dynamics in the Pontchartrain estuary. *Journal of Coastal Research*, *54*(1).

McKee, K.L., Cherry, J.A. (2009). Hurricane Katrina sediment slowed elevation loss in subsiding brackish marshes of the Mississippi River delta. *Wetlands, 29*, 2–15.

Mehta, A., Lee, S-C., and Li, Y. (1994). Fluid mud and water waves: A brief review of Interactive processes and simple modeling approaches. WES Contract Rep. No. DRP-94-4*, U.S. Army Corps of Engineers Waterways Experiment Station, Vicksburg, MS*.

Meselhe, E., McCorquodale, J.A., Shelden, J., Dortch, M., Brown, T.S., Elkan, P., Rodrigue, M.D., Schindler, J.K., Wang, Z. (2013). Eco-hydrology component of Louisiana's 2012 Coastal Master Plan: Mass-Balance Compartment Model. In: Peyronnin, N.S. and Reed D.J. (eds.), Louisiana's 2012 Coastal Master Plan Technical Analysis. *Journal of Coastal Research, 67,* 16-28.

Meselhe, E.A., Arceneaux, J.C., and Waldon, M.G. (2010). Water budget model for a remnant northern Everglades wetland. *Journal of Hydraulic Research*. *48*(1),100-105. doi:01.1080/00221680903568634

Mikeš, D., and Manning, A. (2010). Assessment of flocculation kinetics of cohesive sediments from the Seine and Gironde estuaries, France, through Laboratory and Field Studies. *Journal of Waterway, Port, Coastal and Ocean Engineering,136*(6), 306-318.

Moskalski, S.M., and Sommerfield, C.K. (2012). Suspended sediment deposition and trapping efficiency in a Delaware salt marsh. *Geomorphology,* 139-140,195-204.

Neumeier, U. and Ciavola, P. (2004). Flow resistance and associated sedimentary processes in a *Spartina maritime* salt-marsh. *Journal of Coastal Research, 20*, 435-447.

Nyman, J.A., Crozier, C.R., and DeLaune, R.D. (1995). Roles and patterns of hurricane sedimentation in an estuarine marsh landscape. *Estuar Coast Shelf Sci., 40*, 665–679.

Park, E.J., Yu, K.B., Ku, C.Y., Psuty, N.P., Kim, D., and Shin, Y.H. (2012). Short-term sedimentation processes and accretion rates in the Sunchon Bay estuarine marsh, South Korea. *Journal of Coastal Research, 28*, 1057-1067.

Philips, O.M. (1966). *The dynamics of the upper ocean*. Cambridge University Press.

Roblin, R. (2008). *Water quality modeling of freshwater diversions in the Pontchartrain estuary*. (Unpublished master's thesis). University of New Orleans, New Orleans, LA.

Rossby, C.G., and Montgomery, D.B. (1935). The layer of frictional influence in wind and ocean currents.

Roth, W.B. (2009). *The development of a screening model for the Arthur R. Marshall Loxahatchee National Wildlife Refuge*. (Master's thesis). University of Louisiana at Lafayette, Lafayette, LA.

Rouse, L.J., and Coleman, J.M. (1976). Circulation observations in the Louisiana Bight using Landsat Imagery. *Remote Sensing of Environment*, 5, 55-66.

Schubel, J.R. (1968b). Suspended sediment of the northern Chesapeake Bay. *Chesapeake Bay Institute Tech, 35*, 264.

Sheng, Y.P., and Lick, W. (1979). The transport and resuspension of sediments in a shallow lake. *Geophysical Res, 84*, 1809-1826.

Simons, D.B., and M.L. Albertson.(1960). Uniform water conveyance channels in alluvial material. *Journal Hyd. Div., ASCE, 86 (HY5),* 33-71.

Song, K., Wang, Z., Blackwell, J., Zhang, B., Li, F., Zhang, Y., and Jiang, G. (2001). Water quality monitoring using Landsat Thematic Mapper data with empirical algorithms in Chagan Lake, China. *Journal of Applied Remote Sensing*, 5, 053506-1-053506-16.

Trosclair, K.J. (2013). *Wave transformation at a saltmarsh edge and resulting marsh edge erosion: Observations and modeling*. (Unpublished master's thesis). Department of Geological Sciences, University of New Orleans, New Orleans, LA.

Trzaska, J. R., Miller, B., McKee, and Powell, R. (2002). Monitoring sediment resuspension events in shallow aquatic systems using remote sensing and numerical models. *Seventh Thematic Conference, Remote Sensing for Marine and Coastal Environments.* Miami, FL.

Tsihrintzis, V.A. and Madiedo, E.E. (2000). Hydraulic resistance determination in marsh wetlands. *Water Resources Management,14*, 285-309.

Turner, R.E., Baustian, J.J., Swenson, E.M., and Spicer, J.S. (2006). Wetland sedimentation from hurricanes Katrina and Rita. *Science*. *314*(5798), 449-452.

Tweel, A.W., and Turner, R.E. (2012). Landscape-scale analysis of wetland sediment deposition from four tropical cyclone events. *PLOS ONE* 7(11), e50528.

U.S. Army Corps of Engineers. (1984). *Shore Protection Manual.* U.S. Government Printing Office, Washington, DC.

U.S. Army Corps of Engineers. (2002). *Coastal Engineering Manual. Engineer Manual 1110-2-1100*, U.S. Army Corps of Engineers, Washington, DC.

U.S. Environmental Protection Agency. (2014). Water Quality Analysis Simulation Program (WASP). Retrieved from http://www.epa.gov/athens/wwqtsc/WASP.pdf

van Rijn, L.C. (1984a). Sediment transport, Part I: Bed load transport, *Journal of Hydraulic Engineering*, ASCE, *10*.

van Rijn, L.C. (1984b). Sediment Transport, Part II: Suspended load transport. *Journal of Hydraulic Engineering*, ASCE, *11*.

van Rijn, L.C. (1984c). Sediment pick-up functions. *Journal of Hydraulic Engineering,* ASCE, *10*.

van Rijn, L.C. (2007a). Unified view of sediment transport by currents and waves. I: Initiation of motion, bed roughness, and bed-load transport. *Journal of Hydraulic Engineering*, *133*(6), 668-689.

van Rijn, L.C. (2007b). Unified view of sediment transport by currents and waves. II: Suspended transport. *Journal of Hydraulic Engineering*, 133(6), 668-689.

van Rijn, L.C. (2013). Simple general formulae for sand transport in rivers, estuaries and coastal waters. Retrieved from www.leovanrijn-sediment.com

Volpe, V., Silvestri, S., and Marani, M. (2011). Remote sensing retrieval of suspended sediment concentration in shallow waters. *Remote Sensing of Environment*, *115,* 44-54.

Wang, F.C., Lu, T. and Sikora, W.B. (1993). Intertidal marsh suspended sediment transport processes, Terrebonne Bay, Louisiana, U.S.A. *Journal of Coastal Research,* 9, 209-220.

White, W.R., Milli, H., and Crabbe, A.D. (1978). Sediment transport: an appraisal of available methods. *Report No. IT 119, Second Ed.* Hydraulic Research Station, Wallingford, UK.

Williams, H.F.L., and Flanagan, W.M. (2009). Contribution of Hurricane Rita storm surge deposition to long-term sedimentation in Louisiana coastal woodlands and marshes. *J Coastal Res SI*, *56,* 1671–1675.

Williams, H.F.L. (2012). Magnitude of Hurricane Ike storm surge sedimentation: implications for coastal marsh aggradation. Earth Surf Proc. Land 37: 901–906.

Yocum, T., Georgiou, I.Y., Trosclair, K., and Breaux, K. (2013). Do constructed crevasses obey delta laws? Implication for the restoration of the Mississippi River delta. *Proceedings of Basics of the Basin 2013.* New Orleans, LA.

Young, I.R. and Verhagen, L.A. (1996a). The growth of fetch limited waves in water of finite depth. *Part 1. Total energy and peak frequency*. *Coastal Engineering,* 29(1996), 47-78.

Young, I.R. and Verhagen, L.A. (1996b). The Evolution of Wind-Waves in Finite Depth Water. In M.A. Donelan, W.H. Hui and W.J. Plant (Eds.), *The Air-Sea Interface* (pp. 97-104). Toronto: University of Toronto Press.